Coherence and Pattern Analysis of Bipolar EMG-Currents during Running

Master's Thesis in Medical Engineering

submitted
by

Martin Ullrich

born January 11, 1991 in Lohr am Main

Written at

Lehrstuhl für Mustererkennung (Informatik 5)
Department Informatik
Friedrich-Alexander-Universität Erlangen-Nürnberg

in Cooperation with

Human Performance Laboratory, University of Calgary.

Advisor: Prof. Dr. Björn Eskofier (FAU Erlangen-Nürnberg)
Prof. Dr.-med. Jochen Klucken (FAU Erlangen-Nürnberg)
Prof. Dr. Vinzenz von Tscharner (University of Calgary)
Maurice Mohr (B. Sc.) (University of Calgary)

Started: May 15, 2017

Finished: November 15, 2017

Ich versichere, dass ich die Arbeit ohne fremde Hilfe und ohne Benutzung anderer als der angegebenen Quellen angefertigt habe und dass die Arbeit in gleicher oder ähnlicher Form noch keiner anderen Prüfungsbehörde vorgelegen hat und von dieser als Teil einer Prüfungsleistung angenommen wurde. Alle Ausführungen, die wörtlich oder sinngemäß übernommen wurden, sind als solche gekennzeichnet.

Die Richtlinien des Lehrstuhls für Studien- und Diplomarbeiten habe ich gelesen und anerkannt, insbesondere die Regelung des Nutzungsrechts.

Erlangen, den 15. November 2017

Acknowledgements

I would like to thank Prof. Dr. Vinzenz von Tscharner, Maurice Mohr, and Daniel Comaduran Marquez for guiding me through this project. Without their daily help and advice I could not have finished this thesis.

I would like to thank Prof. Dr. Benno Nigg and Sandro Nigg for having me as a visiting student in the Human Performance Laboratory at University of Calgary. The experience I gained during my time in their research group will always help me to be a better individual, professionally and personally.

I would like to thank Heiko Schlarb from adidas AG, who encouraged me to take the opportunity of working on my Master's thesis in Calgary, and Prof. Dr. Björn Eskofier for supervising my thesis from FAU Erlangen-Nürnberg and for the great support during my time as his student.

I would like to thank my parents, my sisters, and my girlfriend Lisa. Their love, trust, and support in all my decision making helped me to go through the whole time of my studies with courage and confidence.

Finally I would like to thank all the friends I made along the journey of my studies in Erlangen and Calgary: Tristan, Philipp, Konrad, Fabi, Pietro, Philipp, Aaron, Fabian, Saša, Fran and many more. Together we went through a lot of hard work, but with the good times we shared it was great fun in the end.

The following text is not just mine, but the result of the collaboration of all people who helped me to get where I am now.

Abstract

Intermuscular synchronization of motor units (MU) in dynamic movements measured by electromyography (EMG) has been a subject of biomechanics research for many years. The results of recent studies give hints for the EMG signal to be generated by a central control system and not to act as a random signal. This study investigated EMG data from vastus medialis (VM) and vastus lateralis (VL) that were recorded during running. Coherence and pattern analysis methods were applied to the data to look for 1) similarities in the signals of the two muscles within a sequence of steps, and 2) groups of signal patterns within the data of a single muscle. The EMG of the vasti muscles from twelve healthy male subjects, who performed at least 1000 steps each, were analyzed. A novel current amplifier was developed to measure bipolar EMG-currents. The current signals were compared against the signals measured by a standard bipolar potential amplifier. Intermuscular MU synchronization was quantified by calculating the coherence spectra between the raw EMG signals of the two muscles. The spectra showed significant coherence values for all subjects in various frequency bands. A wavelet transform was applied to the data from the single muscles to generate wavelet intensity patterns (WIP). Principal component analysis (PCA) and agglomerative hierarchical clustering were used to search for groups of steps with similar WIPs. The steps were grouped in clusters showing similar WIPs, where the grouping was based on distinct frequency bands and their timing within the WIPs. The findings for intermuscular MU synchronization and the possible existence of predefined muscle activation patterns within the muscles indicate that the activation strategy of the running steps is centrally controlled.

Übersicht

Intermuskuläre Synchronisierung von motorischen Einheiten bei dynamischen Bewegungen, gemessen mit Hilfe von Elektromyographie(EMG), ist seit vielen Jahren ein Gegenstand der Biomechanikforschung. Die Ergebnisse neuer Studien geben Hinweise darauf, dass das EMG-Signal von einem zentralen Kontrollsystem generiert wird und sich nicht wie ein stochastisches Signal verhält. Diese Studie untersuchte EMG-Daten von Vastus medialis (VM) und Vastus lateralis (VL), die beim Laufen aufgenommen wurden. Kohärenz- und Musteranalysemethoden wurden auf die Daten angewendet um 1) Ähnlichkeiten in den Signalen der beiden Muskeln innerhalb einer Schrittsequenz und 2) Gruppen von Signalmustern innerhalb der Daten eines einzelnen Muskels zu suchen. Elektromyogramme der Vasti Muskeln von zwölf gesunden männlichen Probanden, die jeweils über 1000 Schritte liefen, wurden analysiert. Ein neuartiger Stromverstärker wurde entwickelt um bipolare EMG-Stromsignale zu messen. Die Stromsignale wurden mit den Signalen, die mit einem etablierten bipolaren Potentialverstärker gemessen wurden, verglichen. Intermuskuläre Synchronisierung von motorischen Einheiten wurde mit Hilfe von Kohärenzspektren zwischen den EMG-Rohsignalen der beiden Muskeln quantifiziert. Die Spektren zeigten signifikante Kohärenzwerte für alle Probanden in mehreren Frequenzbändern. Eine Wavelettransformation wurde auf die Daten der einzelnen Muskeln angewendet um Wavelet-Intensitäts-Muster (WIM) zu erzeugen. Principal Component Analyse (PCA) und agglomerierendes hierarchisches Clustering wurden genutzt um Gruppen von Schritten mit ähnlichen WIM zu suchen. Die Schritte wurden zu Clustern mit ähnlichen WIM gruppiert, wobei die Gruppierung auf bestimmten Frequenzbändern und deren zeitliches Auftreten innerhalb der WIM basierte. Die Erkenntnisse hinsichtlich intermuskulärer Synchronisierung von motorischen Einheiten und der möglichen Existenz von vordefinierten Muskelaktivierungsmustern innerhalb der Muskeln deuten darauf hin, dass die Aktivierungsstrategie der Schritte beim Laufen zentral kontrolliert wird.

Contents

Chapter 1

Introduction

Muscle activity affects many aspects of human locomotion [Nig10]. One possibility to determine the muscle activity responsible for a specific task is to measure the electromyographic (EMG) signal of the muscles during the execution of that task. Current research is aiming to develop methods to investigate the question if thigh muscles of humans – especially vastus lateralis (VL) and vastus medialis (VM) – show a degraded synchronization of the muscle activity after a knee injury. This could alter the forces that are acting across the knee joint, which may lead to tissue degradation over time and possibly knee osteoarthritis [Mel05b]. Considering this background, there are many open possibilities regarding the enhancement of the usage of EMG in terms of signal acquisition and data analysis. In the following, several of these aspects will be introduced.

1.1 Task dependent motor unit synchronization

Humans are capable of executing complicated tasks and movements requiring a precise control of the muscles that are used to generate force and movements [DL97]. Neuro-muscular control mechanisms are responsible for the regulation of muscle activity. This activity is investigated by measuring signals related to the excitation of motor unit action potentials (MUAP). The resulting signal is measured on the skin as a surface EMG, which is the result of a superposition of MUAPs [Kon06, Sil09]. The precise control of human movements requires the synchronization of the responsible motor units (MU). MU synchronization was defined by De Luca et al. as the tendency of two motor units to fire at fixed time intervals with respect to each other and more often than would be expected for independent firing [DL93]. The measurement of MU synchronization offers a possibility that allows a functional examination of the intact central nervous system during voluntary contractions of the muscle [Sem02]. One can differentiate between intra- and

intermuscular MU synchronization, describing the synchronized MUs within a muscle or between two or more muscles.

An established method for the evaluation of MU synchronization is the computation of cross-correlation of the discharge times of two concurrently active motor units [Sem02]. Thus, correlation was used to demonstrate task dependency of intramuscular MU synchronization. Individual muscle compartments of gastrocnemius medialis showed a higher correlation for a dynamic calf rising movement than while balancing in a tiptoe position [vT14a].

Coherence, the frequency domain equivalent of cross-correlation analysis, has been successfully applied to show a significant association between MU firings within one muscle as well as between muscles [Far93]. Coherence analysis supported the finding of task dependent intramuscular synchronization of MUs during vertical calf rising movements between individual muscle compartments of gastrocnemius medialis [vT14b].

Mellor et al. reported high degree of synchronization of MU firings also between several muscles that are involved in the same movement [Mel05a]. Task dependency of intermuscular MU synchronization of vastus medialis (VM) and vastus lateralis (VL) using coherence analysis was shown in monopolar EMG-current measurements for different types of squats by Mohr et al. [Moh15].

1.2 Pattern analysis in EMG

Recent results regarding MU synchronization indicate that the EMG signal is generated by a certain central control system and does not act as a random signal as suggested previously [Rea06, Geo03]. Even though specific features of EMG signals do not appear when looking at the raw signal, wavelet based time-frequency analysis has been successfully applied to EMG signals [vT00] to reveal spectral, timing, and intensity characteristics of muscle activation patterns. Using this technique, EMG signals from tibialis anterior could be used to distinguish between data that was recorded while running in shoes versus barefoot [vT03b].

However, due to the complexity of the EMG time-frequency patterns, the visual comparison of patterns from multiple trials of one individual can typically not reveal the underlying control mechanisms. Therefore, pattern analysis and machine learning methods have to be applied to assign the wavelet transformed EMG signal to a specific movement condition [vT09]. Von Tscharner described the representation of an EMG intensity pattern as a vector in a high dimensional feature space, also called pattern space [vT02]. Application of pattern analysis methods, including principal component analysis (PCA) and whitening of the dimensionality reduced data, allowed

the classification of multi-muscle-patterns from male and female runners [vT03a] and from shod and barefoot runners [vT09].

In terms of healthcare applications, EMG signals could be used to recognize pathologic patients with a support vector machine [Gül05]. Wavelet transformed multi-muscle EMG patterns were used to classify post-operative female total knee arthroplasty (TKA) patients and healthy controls [Kun15].

A common criterion of the previously mentioned studies was the fact that there was labeled training data available and thus supervised classification methods could be used. In contrast, unsupervised learning approaches seek to discover groups of similar samples within an input data set if grouping variables are unknown. These types of algorithms belong to the group of clustering algorithms [Bis06]. A k-means clustering based method for the decomposition of EMG signals in single MUAPs was reported in [Nin15]. Christodoulou et al. applied unsupervised learning methods to EMG signals for the diagnosis of neuromuscular disorders [Chr99]. Hierarchical clustering was used to assess biometric expressions of students within an educational game based on skin conductance, heart rate, and EMG in [Ame06]. One advantage of the hierarchical approach in this study was that the number of clusters did not have to be determined beforehand, which is always useful if the result is not predictable or may vary between subjects.

1.3 EMG signal acquisition

The established technology for EMG signal acquisition is the bipolar potential amplifier, which is a high impedance differential amplifier [Kon06]. Bipolar potential measurements, however, suffer from intra-electrode cross talk, caused by the low resistance between the electrodes [vT13]. The effect of this cross talk could be observed in a dampening of the amplitude of the EMG signal due to sweat accumulation under surface EMG electrodes, where sweat as a conductor is decreasing the resistance between the electrodes [AE12]. Facing this problem, von Tscharner et al. introduced the concept of a current based measurement [vT13]. This technique was further improved and successfully used in several studies for EMG measurements in kinesiology [vT13, vT14a, vT14b, Nan14, Moh15, CM16]. The proposed method uses a transimpedance amplifier (TIA), which is a current-to-voltage converter [vT13, Tie16]. One advantage of this approach is that the electrodes remain on ground potential, with the result that lateral currents are eliminated and intra-electrode cross talk can be prevented. As a great benefit, current based measurements can also be obtained under water. Whitting et al. reported no loss of signal amplitude when comparing EMG signals measured under water with those recorded during a

muscle contraction in air [Whi14]. Outgoing from this finding, the principle of monopolar current measurements was successfully used for the development of an ECG sensor for the application under water [Lau16].

However, the EMG current amplifiers in the previously mentioned studies were built to measure signals in a monopolar configuration [vT13, Nan14, CM16]. They had thus limitations related to the lack of common mode rejection (CMR): Elimination of signal contamination caused by sources in the environment or motion artifacts is not provided in a monopolar measurement [CM16].

1.4 Patent research

There are several patented systems existing that are related to the topic of EMG and the corresponding signal analysis (Appendix B). In Appendix B.1 an integrated movement analysis system is proposed by Cusimano et al. This system uses EMG in combination with range of motion and functional capacity testing to monitor any muscle group in the human body. The system includes a software program to produce comparative analytical data. The invention that was patented by Church et al. (Appendix B.2) is more focused on the application of EMG as a feedback instrument for exercise training. The system is able to record the intensity of the exercise using an electromyographic sensor, and a built in clock for measuring time intervals of the exercises. Whereas the first to presented patents are directly related to health care and kinesiology, the idea proposed by Tan et al. (Appendix B.3) is using wearable EMG based controllers for a human-computer interface. The controller includes a plurality of EMG sensors that are integrated in an armband. The patent review reveals that EMG is used in various applications from backgrounds more or less related to health care and sports.

1.5 Purpose of the thesis

The literature review shows that there are several approaches to make use of EMG for the investigation of the neuro-muscular control system of the human body. Regarding MU synchronization the movement tasks in many previous studies (vertical calf rising, squats) were chosen to have well defined conditions and an easy measurement setup. These movements, however, are not directly related to the daily life activities of many humans. On the other hand, endurance running has become a very popular exercise for many people over the last years [CR16]. In previous studies, EMG signals acquired during running were used for the purpose of supervised classification

of different conditions. The findings about intermuscular MU synchronization supported the general idea of non-random EMG signals. They thus lead to the question if there might as well be similar signal patterns within one muscle when observing EMG signals over time within a certain condition, for example steady-state running. Repeated signals would show up in certain classes of patterns. As described before, the monopolar current setup that has been used in previous studies, as well as the established bipolar potential amplifier might not be the ideal instruments for the measurement of EMG during running.

Thus, the purpose of this thesis was to find an answer on the question if human beings use preset muscle activation patterns or if the patterns for every running step are unique. Based on the possible issues with available signal acquisition devices, a bipolar current amplifier was developed. This approach was supposed to add the advantage of CMR for the rejection of motion artifacts to the successfully developed current amplifiers. The new device could be used in a running study to collect data from two muscles, VM and VL. Coherence and pattern analysis methods were then applied to the data to look for:

1. Similarities in the signals between the muscles within a sequence of running steps.
2. Groups of signal patterns within the data of a single muscle from all running steps.

1.6 Hypotheses

The following hypotheses were developed for the study:

H1: Different muscles, that are involved in a specific task, show similar EMG signal patterns when performing this task.

H2: For every human there is an individual finite number of task-specific EMG signal patterns within one muscle.

In the present thesis the generic *task* in both hypotheses was steady-state treadmill running.

1.7 Outline

The remainder of the thesis is organized as follows: Chapter 2 provides basic information on EMG, different recording systems, and the related electronics. In Chapter 3 the development and evaluation of the bipolar current amplifier are described. The running study, including methodology, results, and their discussion are presented in Chapter 4. Finally, Chapter 5 provides a conclusion of the thesis with open questions that should be answered in future studies.

Chapter 2

Fundamentals

In the following sections the relevant background regarding EMG, required electronic systems, and instrumentation approaches will be discussed. The information of this chapter will be used in the following chapters, where different methods for the analysis of EMG data will be used to investigate the hypotheses mentioned in the introduction.

2.1 Electromyography

EMG is an experimental technique with the purpose of recording and analyzing myoelectric signals, where myoelectric signals are formed by physiological variations in the state of muscle fiber membranes [Kon06]. EMG signals have been studied intensively as they offer a window into the function of the muscles, the spinal chord, and the brain, the responsible contributors to human movements [Wol96].

Motor units (MUs) are the smallest functional entity to describe the neural control of the muscular contraction process [Kon06]. They consist of the cell body and dendrites of a motor neuron, the multiple branches of its axon, and the muscles fibers that are innervated by it [Eno88]. A schematic of a MU is presented in Fig. 2.1. The description as a unit indicates that all muscle fibers of a single MU act together as one within the innervation process [Kon06]. Muscle fibers are excitable through neural control due to a resting potential. The potential difference of about - 70 mV is produced by the different ionic concentrations between the two sides of the cell membrane [Kon06]. In resting condition there is a higher concentration of Na^+ ions outside of the cell compared to the inside. The opposite is true for K^+ ions that are higher concentrated in the inside of the cell compared to the outside [Spe08].

Induced by a stimulus of the central nervous system, the diffusion characteristics of the muscle

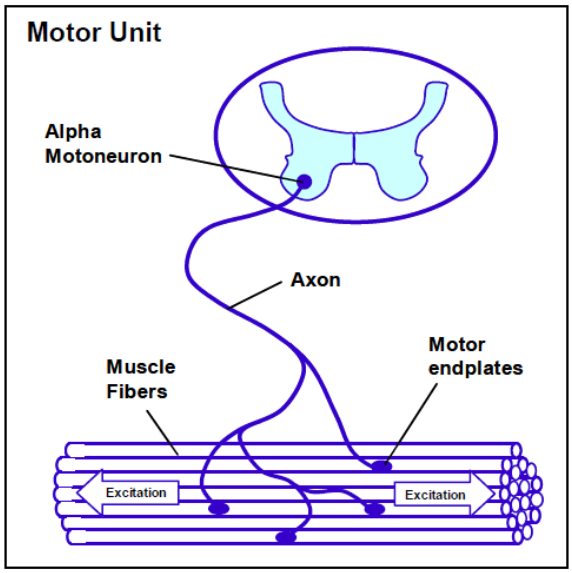

Figure 2.1: Schematic of a motor unit [Kon06].

fiber membrane are briefly modified and Na^+ can flow into the cell [Kon06]. If the Na^+ influx reaches a certain threshold level, a muscle fiber action potential is generated by the depolarization of the membrane. The potential of the cell is briefly increased up to $+40$ mV. The overshoot to the positive potential is followed by the repolarization and the hyperpolarization period of the membrane, before it reaches its resting state again [Spe08]. The progress of an action potential is shown in Fig. 2.2.

All muscle fibers within a MU are innervated by the same motorneuron. Hence, all the muscle fibers within the MU are activated simultaneously and the summed electrical activity is called a motor unit action potential (MUAP) [Sil09]. The MUAP can now be recorded from the body as an EMG signal using electronic instrumentation. Two commonly used techniques are applied: intramuscular or surface EMG measurements. For intramuscular measurements a needle electrode is punctured through the skin and placed into the muscular tissue. This invasive technique is a proper method for the acquisition of individual MU activity but not suitable for the recording of muscle activity in dynamic tasks. Surface EMG measurements on the other hand, are non-invasive and provide an EMG signal that is more representative for the whole muscle activity. Here an adhesive electrode, made of flexible material and equipped with a conductive Ag/AgCl solution is attached to the skin after proper preparation [Kon06]. Surface electrodes are located further away from the muscle fibers as needle electrodes, hence the recorded signals are affected by dispersion through the adjacent tissues [CM16]. However, due to the easier handling and the non-invasive character, surface EMG measurements are preferred for the application in kinesiology studies.

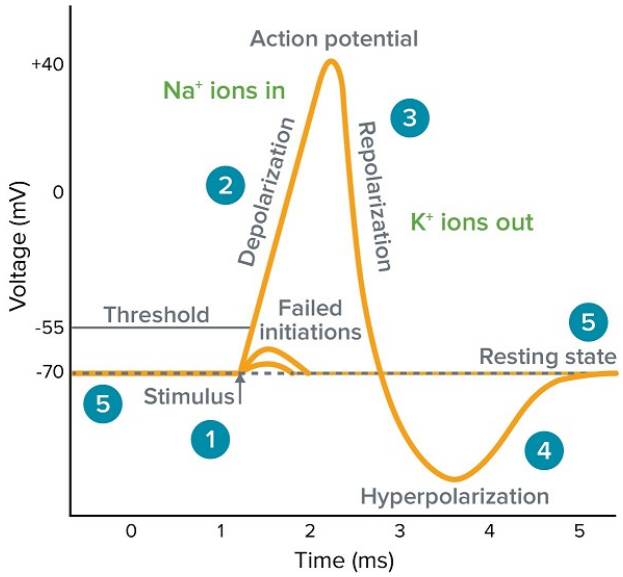

Figure 2.2: Example for the signal course of an action potential [Dev17].

2.2 Electronics

After the introduction of the generation and transduction of the EMG signal, in the following electronic basics for the amplification of EMG signals using operational amplifiers (OPAMPs) will be described.

Ideal operational amplifier

An OPAMP is a multistate DC-voltage amplifier, that is produced as an integrated circuit [Tie16]. An ideal OPAMP has several basic characteristics [CM16, Tie16]:

1. Infinite open loop voltage gain
2. Infinite input impedance
3. Zero output impedance
4. Infinite bandwidth
5. Zero input offset voltage

In general an OPAMP is outputting the amplified difference of the input voltages [Tie16]. It is therefore performing a differential measurement of the input signals. Any interference with the ground potential will affect both of these signals equally, which makes differential measurements highly immune to external interference and noise [CM16]. The feature of not amplifying those parts of the signal that are common in both inputs is called common mode rejection (CMR) [Tie16].

As an ideal OPAMP is supposed to offer infinite open loop voltage gain, a small difference at the two inputs generates a large difference at the output. Thus, a feedback loop is used to keep the voltage difference between the inputs to zero [CM16].

Transimpedance amplifier

The transimpedance amplifier (TIA) is a specific circuit using one OPAMP and is also known as a current-to-voltage converter [Tie16]. A TIA is suitable for the use of sensors which have a current response that is more linear than a voltage response [CM16]. A schematic for a TIA is shown in Fig. 2.3. The TIA consists of a feedback resistor R_f and capacitor C_f. Because of the high

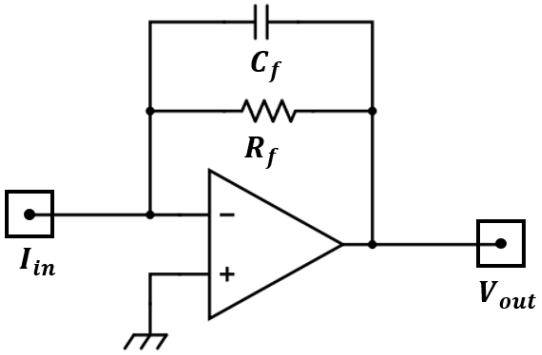

Figure 2.3: Schematic of a TIA.

impedance input of the OPAMP all current I_{in} will go through R_f and C_f. The transfer function for the TIA is given by [Ram09]:

$$V_{out} = \frac{-R_f}{1 + sC_fR_f} \cdot I_{in}. \tag{2.1}$$

The capacitor C_f is affecting the bandwidth of the TIA by allowing only low frequencies to pass [CM16].

2.3 EMG systems

Recording EMG signals by measuring potentials on the skin is a standard method to detect muscle activity in a non-invasive way. The potentials are typically measured with a bipolar high impedance differential amplifier [Kon06]. Hence, the EMG signal is obtained by assessing the potential differences between the bipolar surface electrodes. In contrast, recently monopolar

current measurements have been suggested by von Tscharner et al. [vT13]. In the following the two principles of bipolar potential and monopolar current will be discussed and the idea for a bipolar current amplifier will be introduced.

2.3.1 Bipolar potential amplifier

In bipolar potential EMG the principle measurement is a subtraction between the potentials Φ_1 and Φ_2 of the bipolar electrodes using an instrumentation amplifier (IA), a special form of a differential amplifier [Nan14]. A measurement of the differential of the MUAP is possible, if the two electrodes are aligned with the direction of the muscle fibers. The quality of the approximation of the MUAP differential is related to the inter-electrode distance: the closer the electrodes are placed, the more accurately the differential can be measured. The general principle of the bipolar potential method is shown in Fig. 2.4.

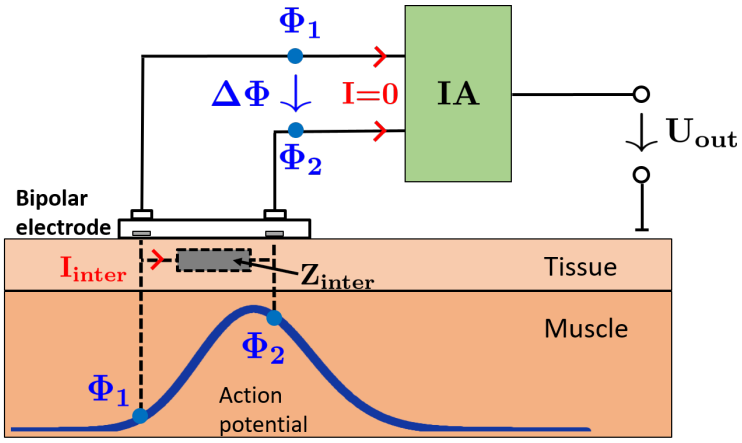

Figure 2.4: Bipolar potential EMG measurement with instrumentation amplifier (IA). The measured EMG signal $\Delta\Phi$ is the differential of the propagating action potential between the probes Φ_1 and Φ_2. As no current can flow into the amplifier, exclusively potentials are measured. Depending on the inter-electrode impedance Z_{inter} an inter-electrode current I_{inter} can alter the measured potentials. Figure adopted and modified from [Nan14].

Due to the high input impedance of the potential amplifier, negligible current flows into the amplifier and the potentials from the skin surface remain unaltered [Nan14]. Furthermore, the bipolar setup makes use of the advantages of the previously described CMR: signals that are common to both inputs of the amplifier (for example 50 Hz or 60 Hz line frequency contamination or motion artifacts) are eliminated, whereas differences in the input signals will be amplified.

Caused by the potential difference between the two measurement points on the skin, there is a lateral current I_{inter} flowing, depending on the inter-electrode impedance Z_{inter}. The lateral

current is also called intra-electrode cross talk [vT13] and it alters the measured potentials in a non-predictable way. Z_{inter} is specifically low in the case of perspiration, allowing a high lateral current. As a result, sweat accumulation under surface EMG electrodes dampens the signal amplitude [AE12]. As subjects are likely to sweat in many studies in the area of sports and healthcare, this issue has to be taken into consideration.

2.3.2 Monopolar current amplifier

One way to overcome the previously described limitations caused by intra-electrode cross talk is the measurement of currents instead of potentials. Monopolar current amplifiers have been successfully developed and used in different studies investigating intra-muscular and inter-muscular coherence [vT13, Nan14, CM16]. EMG-currents can be measured using a TIA (Section 2.2). As a TIA amplifies an input current and converts it into voltage, it is further referred to as a current amplifier. The current amplifier is able to remove or inject electronic charges at the skin surface, such that the potential at the respective electrodes will always stay on reference potential Φ_0. Thus, there will be no potential difference between different electrodes causing an inter-electrode current to flow. The general principle of the monopolar current amplifier is shown in Fig. 2.5.

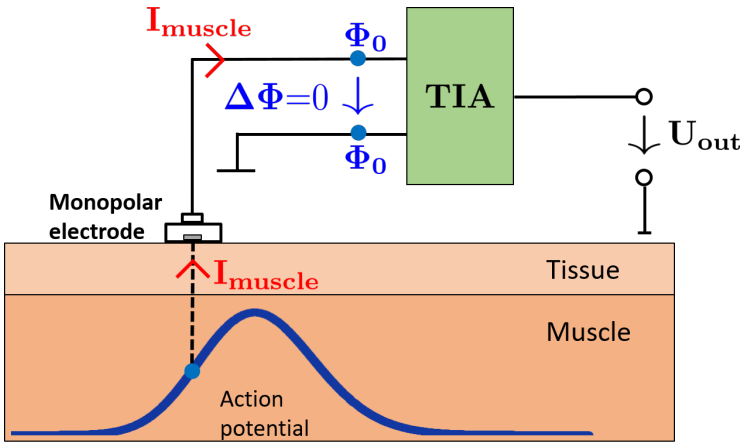

Figure 2.5: Monopolar current EMG measurement with a transimpedance amplifier (TIA). The monopolar electrode is on reference potential Φ_0. The measured current I_{muscle} is caused by the MUAP during muscle contraction. The output potential U_{out} is depending on the internal feedback resistor of the amplifier as described in Section 2.2. Figure adopted and modified from [Nan14].

One of the advantages of the current amplifier was shown by Whitting et al. [Whi14], who reported that EMG-current measurements under water, which is the extreme case for perspiration, did not show loss of signal amplitude, comparing the signals to measurements made in air.

The major drawback of the monopolar current amplifier compared to the bipolar potential amplifier is the lack of CMR. Any noise or motion artifact that is present at the input will thus be amplified in the resulting output signal.

2.3.3 Bipolar current amplifier

In the two previous sections, several advantages and disadvantages of the available EMG acquisition technologies were described. The reasonable conclusion would be to use the advantage of the bipolar setup (CMR) and of the current measurement (no intra-electrode cross talk) and combine them to a bipolar current amplifier. One possible way to design a bipolar current amplifier is to use two TIAs at a bipolar input interface. The two input currents are converted to voltage and the difference of them is amplified using an IA. The bipolar current amplifier with this setup is therefore a differential TIA, the principle is shown in Fig. 2.6.

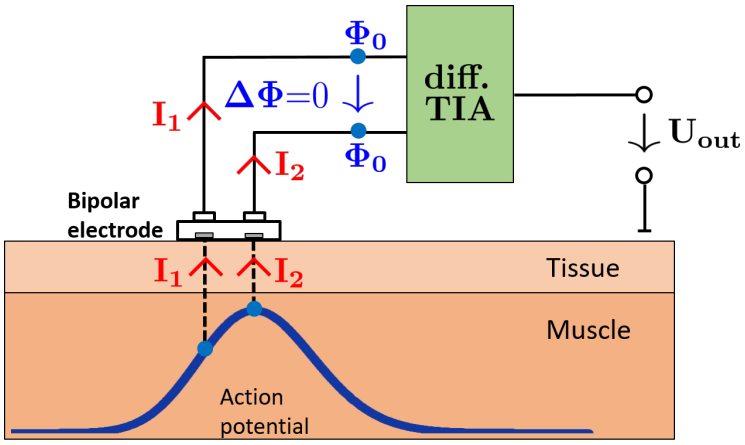

Figure 2.6: Bipolar current EMG measurement with a differential TIA. Both of the bipolar electrodes are on reference potential Φ_0. As there is no potential difference between the measurement points, no intra-electrode current will flow. Thus, a closer inter-electrode distance as for the bipolar potential amplifier can be used without altering of the signal.

One major advantage of this technology is the possible use of bipolar electrodes with a close inter-electrode distance. As described before, in a current measurement the electrodes stay on reference potential such that there will be no intra-electrode cross talk, even in the presence of sweat and for a short distance between the electrodes. In the following chapter the development and implementation of a bipolar current amplifier will be described in detail.

Chapter 3

Hardware development

With respect to the advantages that were described before, a bipolar current amplifier was designed, implemented, and built. In the following sections the development of the amplifier will be presented.

3.1 Previous work

The principle of using current measurements for the detection of muscle activity was introduced by von Tscharner et al. in 2013 [vT13]. The original system showed limitations in terms of signal filters and inter-muscular cross-talk [Nan14, Moh15, CM16]. Therefore, the original system presented in [vT13] was further developed by Comaduran, who added active high and low-pass filters with a flat frequency response from 10 to 500 Hz, as well as an isolation module that allowed simultaneous recordings from multiple muscles without inter-muscular cross-talk [CM16]. The block diagram of this system is presented in Fig. 3.1.

The design of the EMG-amplifier that is presented in this thesis is mainly based on the previously mentioned systems. All previous systems were built to perform monopolar measurements using a single TIA at the input. However, in Section 2.3 the advantages of bipolar systems were explained. Especially regarding the ability to cancel out common input signals, for example motion artifacts, in the following running study a bipolar approach was required. Hence, for this project a bipolar EMG-current amplifier was developed.

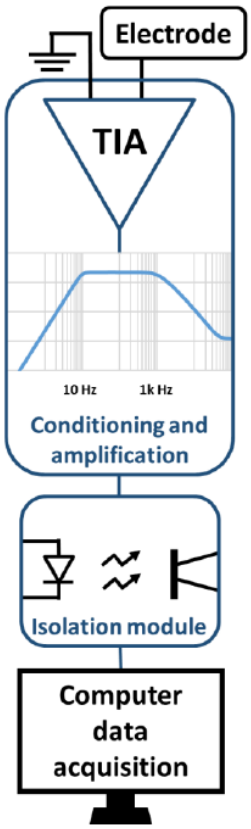

Ag/ Ag-Cl surface EMG electrodes

Trans-impedance amplifier, (current-to-voltage converter)

Butterworth 4^{th} order HPF f_c = 10 Hz

Butterworth 2^{nd} order LPF f_c = 1 kHz

Optical coupling isolation device

Allows to record simultaneously from multiple muscles

12-bit DAQ and acquisition software developed with Matlab®

Figure 3.1: Block diagram of the current amplifier system with design goals from [CM16].

3.2 System design

The new amplifier was supposed to be designed the way that it would have an interface to Comaduran's [CM16] Butterworth signal filters and isolation module. Therefore, only the parts including the monopolar setup for the electrode and the TIA from Fig. 3.1 were changed for the new system proposed in this thesis. The design for the high pass and low pass filter, the isolation module, and the computer data acquisition were adopted from [CM16].

The new front end was designed using TINA-TI 9 (Texas Instruments, Dallas, TX, USA). The electronic schematic for the bipolar current amplifier as well as for the filter section, which is integrated in the same circuit, is shown in Fig. 3.2. Instead of only one TIA for a monopolar measurement as in [CM16], the bipolar amplifier used two TIAs at the input stage, providing two measurement points for a bipolar measurement. Each of the two TIAs at the input offered a current-to-voltage conversion of the current from the input electrode (I_{in}) into an amplified voltage V_{TIA}. The relation between I_{in} and V_{TIA} is proportional to the TIA resistor (R_{TIA}) using Ohm's law [Tie16]:

$$V_{TIA} = I_{in} \cdot R_{TIA} \tag{3.1}$$

The bipolar setup provided two input signals $I_{in,1}$ and $I_{in,2}$. After the conversion at the input stage the two separate voltage signals $V_{TIA,1}$ and $V_{TIA,2}$ were transferred to an instrumentation amplifier (INA128, Texas Instruments, Dallas TX, USA [Tex15]) which only amplified and forwarded the difference of the two input signals. The new front end can therefore be seen as a differential TIA, that took two current signals as inputs and provided one amplified voltage signal V_{out} at the output. This output corresponded to the amplified difference of the two input signals, where the amplification factor (gain G) is depending on the gain resistor R_G used in the instrumentation amplifier [Tie16]:

$$V_{out} = (V_{TIA,2} - V_{TIA,1}) \cdot G \tag{3.2}$$

According to the data sheet of the amplifier [Tex15] the gain equation for the INA128 is given by

$$G = 1 + \frac{50\text{k}\Omega}{R_G}. \tag{3.3}$$

The amplitude of the EMG signal measured by the surface electrode depends on the number of MUs that are located under the sensitive area of the electrode [Kon06]. The magnitude of the signal is therefore dependent on the electrode placement on the skin above the muscle and the

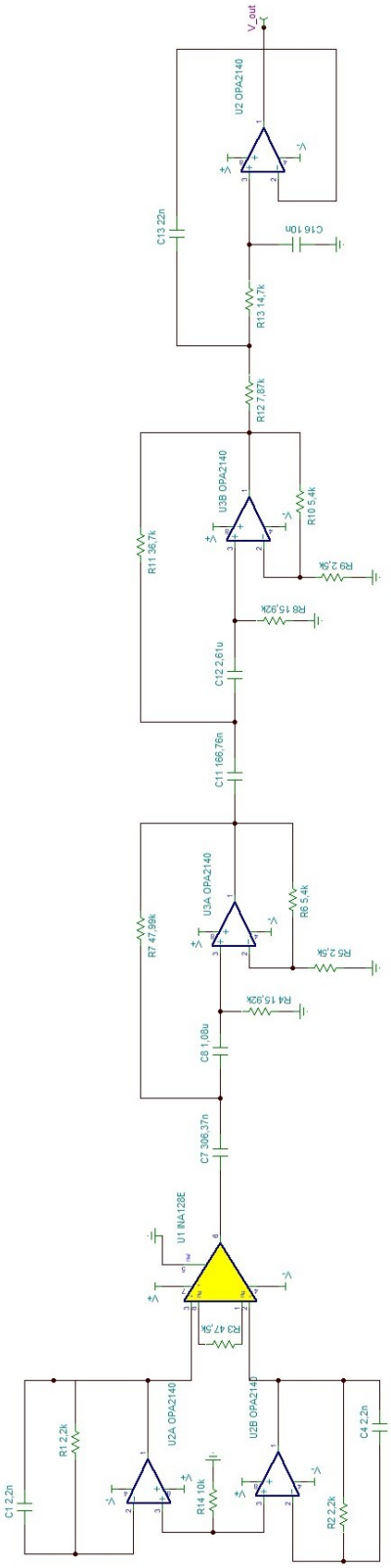

Figure 3.2: Electronic schematic of the bipolar current amplifier circuit.

Table 3.1: Resistor values for the amplification switch of the instrumentation amplifier

Amplification	R_G	G
Low	∞ (no resistor)	1.00
Medium	47.5 kΩ	2.05
High	10.0 kΩ	6.00

underlying muscle structure of the respective subject to be tested. In order to adjust the signal amplitude to the given conditions, a switch was built in to choose between three different resistor configurations for R_G (Table 3.1). The selection of the respective value for R_G provided an appropriate amplification for EMG measurements, where a high, medium, and low amplification were differentiated.

3.3 Simulation

Before implementing the bipolar current amplifier on a breadboard for testing, simulations of the frequency response were performed using TINA-TI 9. According to [Kon06] the relevant frequencies of the EMG signal are those between 10 and 500 Hz. Using the filters presented in [CM16] a flat gain response in the frequencies of interest could be obtained for the three gain values (Fig. 3.3), whereas all lower and higher frequencies were filtered.

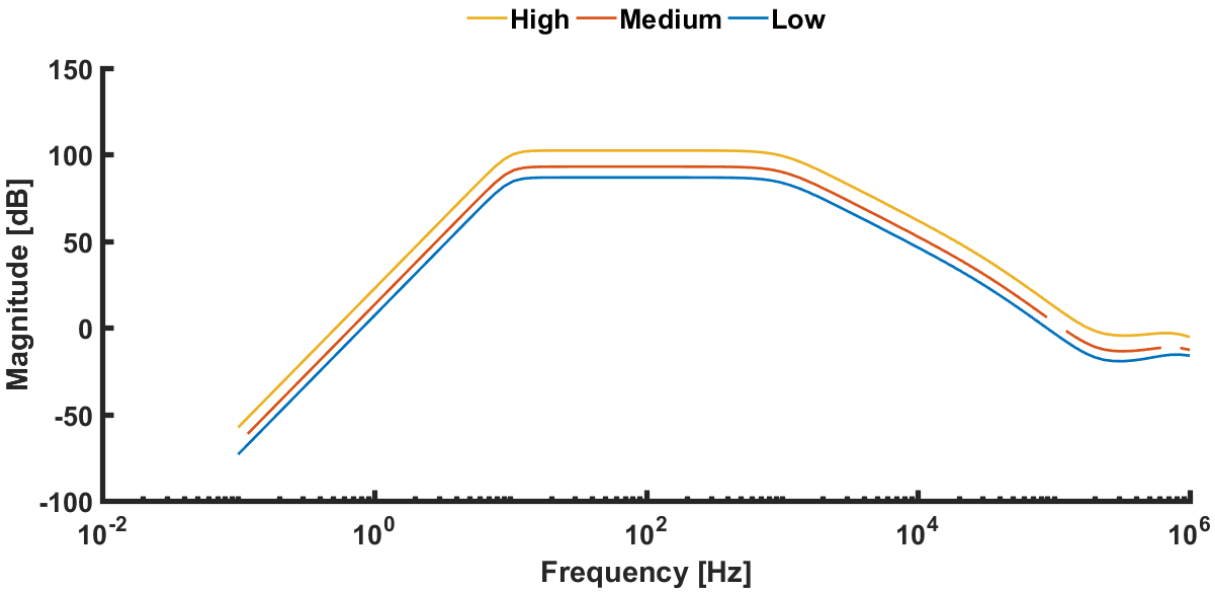

Figure 3.3: Simulated frequency response of the bipolar current amplifier.

3.4 PCB development

In order to design a small size final version of the bipolar current amplifier, the electronic schematics were transferred to the PCB design software Ultiboard 14 (National Instruments, Austin, TX, USA). The circuit for the amplifier was implemented into a dual layer board to reduce the size and make it portable and handy for a running study. The components were chosen in size 0805 which allowed a reduced size while keeping the complexity of the soldering process at an acceptable level. The PCB of the amplifier is shown in Fig. 3.4a.

As the amplifier was supposed to be compatible with the isolation module from [CM16], the output signal was transferred to the isolation module using a mini USB interface. The USB connection was also used as the amplifier's power supply, as the isolation module was connected to 9 V batteries. The amplifier was designed to be used in a running study, where it was in direct contact with the skin of the subjects. The running study would cause the subjects to sweat. For protection of the amplifier from the sweat, the board was surrounded by a 3D printed case. The case had openings for the cables and for the gain selector of the amplifier. As the goal was to measure EMG data from the two muscles VM and VL, two amplifiers were set up to be used in the running study. The final setup of the amplifier is presented in Fig. 3.4b.

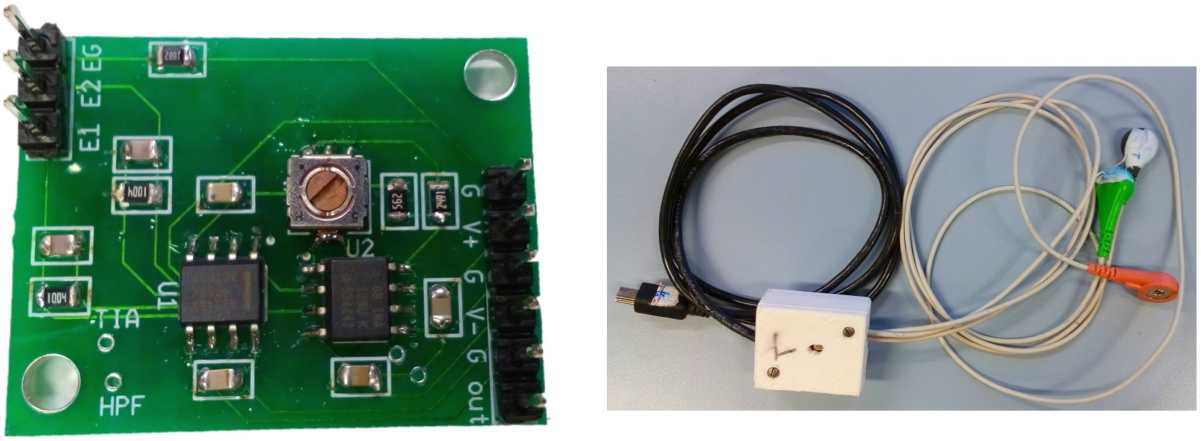

(a) (b)

Figure 3.4: (a) PCB of the bipolar current amplifier. (b) Final setup including the 3D printed case for the PCB and the necessary cables for bipolar EMG measurements and the mini USB connection to the isolation module.

3.5 Characterization

Several tests to measure the performance of the final amplifiers were conducted. The results of these characterization measurements are presented in the following sections.

3.5.1 Frequency response

The frequency response of the current amplifier was measured to ensure that the new amplifier had a flat amplification in the frequencies of interest between 10 and 500 Hz. A trans-conductance amplifier (SR 860, Stanford Research Systems, CA, USA) was used to convert the voltage from a function generator into a current that served as the input for the current amplifier. The frequency response magnitude of the new amplifier was measured for the high gain setting (Table 3.1). The new amplifier showed a constant amplification in the frequencies of interest. The lower and higher frequencies are rejected in the expected way due to the high order filters as described in [CM16].

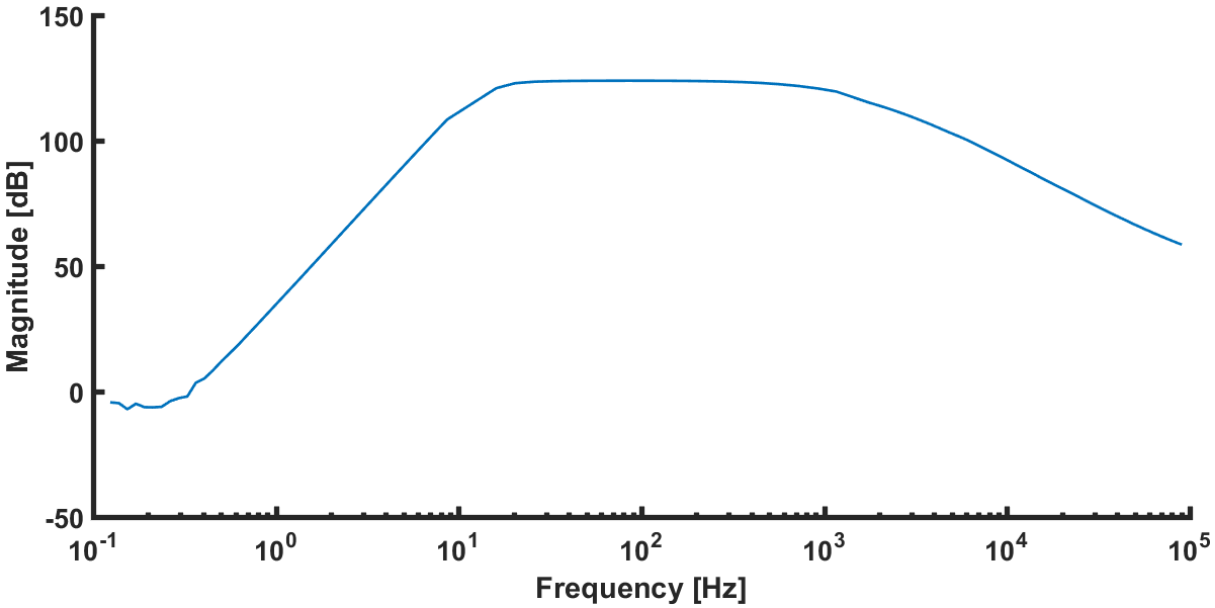

Figure 3.5: Measured frequency response of the bipolar current amplifier.

3.5.2 Input referred noise

The measurement of EMG signals can be affected by different types of electronic noise, for example shot noise, thermal noise, or flicker noise [CM16, Mot93]. This electronic noise can be quantified by measuring the output signal of the amplifier when there is no input to the system

[CM16]. For this experiment the output of the new bipolar current amplifier was measured with a spectrum analyzer (SR760, Stanford Research Systems, CA, USA), that calculates the power spectrum of the measured signal. The amplifier was placed in a Faraday cage and supplied with batteries to avoid introducing noise from a benchtop power supply. The result of the measurement is shown in Fig. 3.6. Compared to the monopolar amplifier in [CM16] the new bipolar current amplifier shows larger noise. This could be further improved by a different setup of the gain values in the different stages of the circuit design in Fig. 3.2. However, the noise values are still orders of magnitude lower than the EMG signals that were supposed to be measured. Therefore, the noise does not have major effects on the output EMG signal.

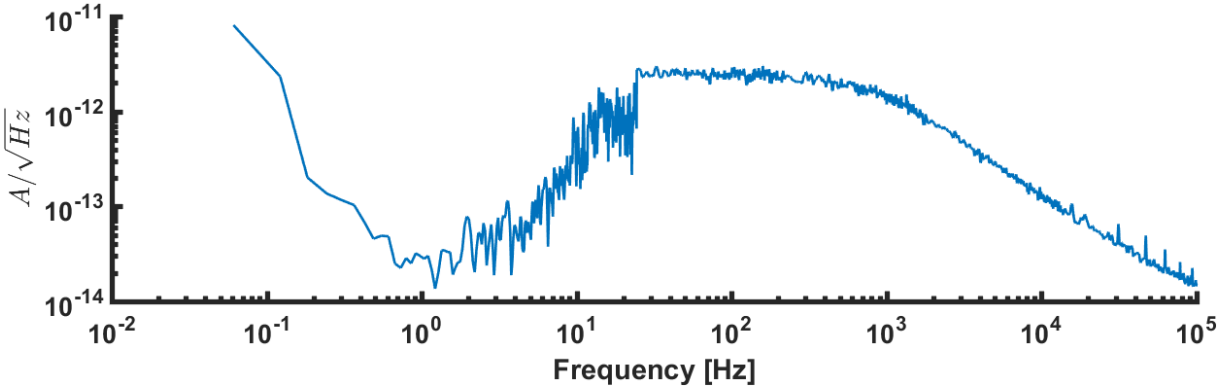

Figure 3.6: Input referred noise for the bipolar current amplifier

3.5.3 Common mode rejection

As explained in Chapter 2 one of the major advantages of a bipolar amplifier is the CMR. The amplifier is supposed to only amplify the difference of the two input signals, signals that are common in both input signals are rejected. A quantitative measure for the CMR is the common mode rejection ratio (CMRR). It describes the ratio of the differential gain A_{d} and the common mode gain A_{cm}. It is often given in dB and can be computed as follows [Tie16]:

$$\mathrm{CMRR}_{dB} = 20 \log_{10} \left(\frac{A_{\mathrm{d}}}{A_{\mathrm{cm}}} \right) \tag{3.4}$$

The CMRR was determined for the new bipolar current amplifier using the same TCA as for the frequency response measurements (SR 860, Stanford Research Systems, CA, USA). The differential gain was measured by connecting one of the two bipolar inputs to the input current of 1 µA peak-to-peak and leave the other one open. For the common mode gain the same signal was

sent to both inputs, it thus divided to 0.5 µA peak-to-peak. The results of the measurements for different frequencies of the input signals are shown in Fig. 3.7. The results show a good CMRR of more than 70 dB in the frequencies of interest between 10 and 500 Hz.

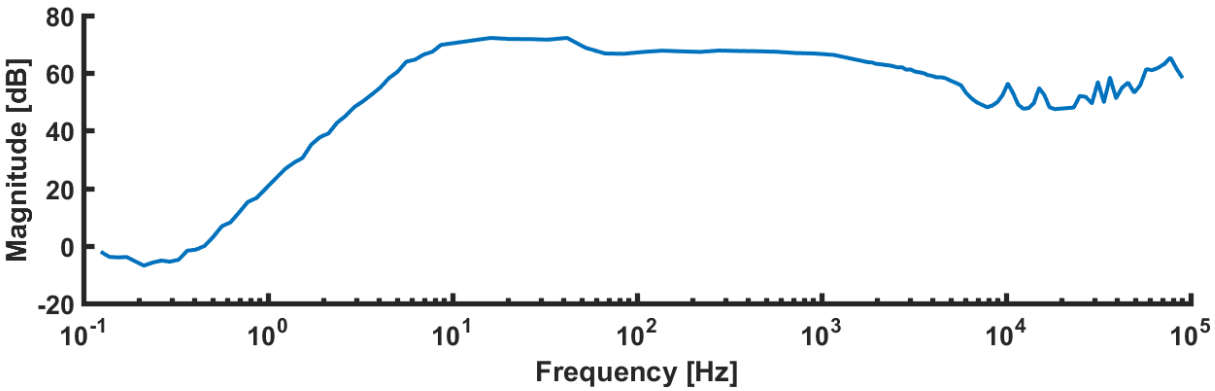

Figure 3.7: Common mode rejection ratio (CMRR) measured for the bipolar current amplifier

3.6 Validation and comparison with potential amplifier

In order to proof the expectations regarding the resistance of the current amplifier against water and sweat, pilot measurements under water and in air as done before in a similar study in [Whi14] were performed. As subjects were expected to sweat during the actual experiment in the following running study, an underwater measurement should simulate the worst-case scenario where the skin and the electrode are completely surrounded by water. The goal was not only to obtain the performance of the bipolar current amplifier under water and in air, but also to compare it with the behavior of the established bipolar potential amplifier in both of these conditions.

3.6.1 Study design

Three male subjects took part in the pilot study. EMG signals were measured on the flexor digitorum muscles located at the right forearm. Both the new bipolar current amplifier and the established bipolar potential amplifier (Biovision, Wehrheim, Germany) were tested in this study. Prior to electrode placement the respective sites were shaved, abraded, and cleaned with alcohol. A bipolar Ag/AgCl electrode with a diameter of 10 mm and inter-electrode distance of 22 mm (Norotrode 20, Myotronics, Kent, WA, USA) was placed in the approximate center of the muscle bellies which were found by palpation during contraction. A ground electrode was placed over the olecranon. Extension cables were applied between the electrodes and the EMG amplifiers. These

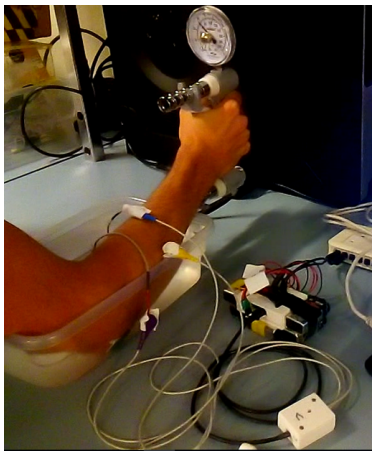

Figure 3.8: Measurement setup for the underwater measurement with the current amplifier.

guaranteed that the electrodes were not touched or moved between the measurements with the current and the potential amplifier. All electrodes and connections with the extension cables were secured with tape, however, there was no waterproof protection for the electrodes or any of the connections. In order to activate the flexor digitorum, subjects were asked to perform isometric contractions using a grip dynamometer according to a predefined experimental procedure. Fig. 3.8 shows the measurement setup for the underwater measurement with the current amplifier. The underwater measurements were performed with the right forearm positioned in a plastic container filled with tap water.

Signals were recorded with a sampling rate of 2400 Hz. For all four conditions (current / potential amplifier, dry / under water) 50 seconds of EMG data were recorded. The subjects and the investigators made sure that the same target force was applied during the contractions. The target force was determined based on subject preference.
The order of tasks for the subjects was as follows:

1. 5 seconds rest
2. 10 seconds **contraction** at 20 kgf for subject 1 and subject 2, at 30 kgf for subject 3
3. 20 seconds rest
4. 10 seconds **contraction** at the same force as before
5. 5 seconds rest

For all subjects the order of conditions was:

1. Current, dry
2. Potential, dry
3. Potential, under water
4. Current, under water

The subjects had sufficient resting time between the conditions to avoid fatigue. The recorded EMG raw signals were passed to a custom notch filter to remove any 60 Hz line frequency contamination. Similar to the work in [Whi14] windows of 8192 samples (3.41 s) containing steady-state, quasi-stationary signals of muscle activation were manually identified and cropped. As explained before the subjects performed two periods of muscle contraction for each experimental condition. Thus, one signal window from each of these two contractions was selected and the average signal of the two probes was used for the further analysis. In order to assess the effects of the experimental conditions, the sum of EMG-power over time was computed, which is equal to the signal energy. Similar as in [Whi14] the square root of the energy was used as the measure for the EMG-magnitude in $[\sqrt{\mathrm{V}^2 \cdot \mathrm{s}}]$. For each subject the respective absolute EMG-magnitude values were normalized to the value for the dry condition. This was done separately for the current and the potential amplifier measurement.

3.6.2 Results

Fig. 3.9 shows the raw data of one subject for the measurements in all four conditions. Each of the four graphs show 50 seconds of data that were recorded per condition with the two periods of isometric contraction. The result of the EMG-magnitude calculation as described in Section 3.6.1 is presented in Table 3.2. The change of the EMG-magnitude after normalization to the dry condition is shown in Fig. 3.10. The signal magnitude increased by 23 to 94 % for the current measurements and it decreased by 77 to 87 % for the potential measurements.

Table 3.2: Absolute values for the EMG-magnitude $[\sqrt{\mathrm{V}^2 \cdot \mathrm{s}}]$ for all subjects during all conditions

Subject	**C. dry**	**C. wet**	**P. dry**	**P. wet**
1	1.59	1.95	16.28	3.89
2	0.45	0.64	6.59	1.34
3	0.76	1.47	21.39	2.83

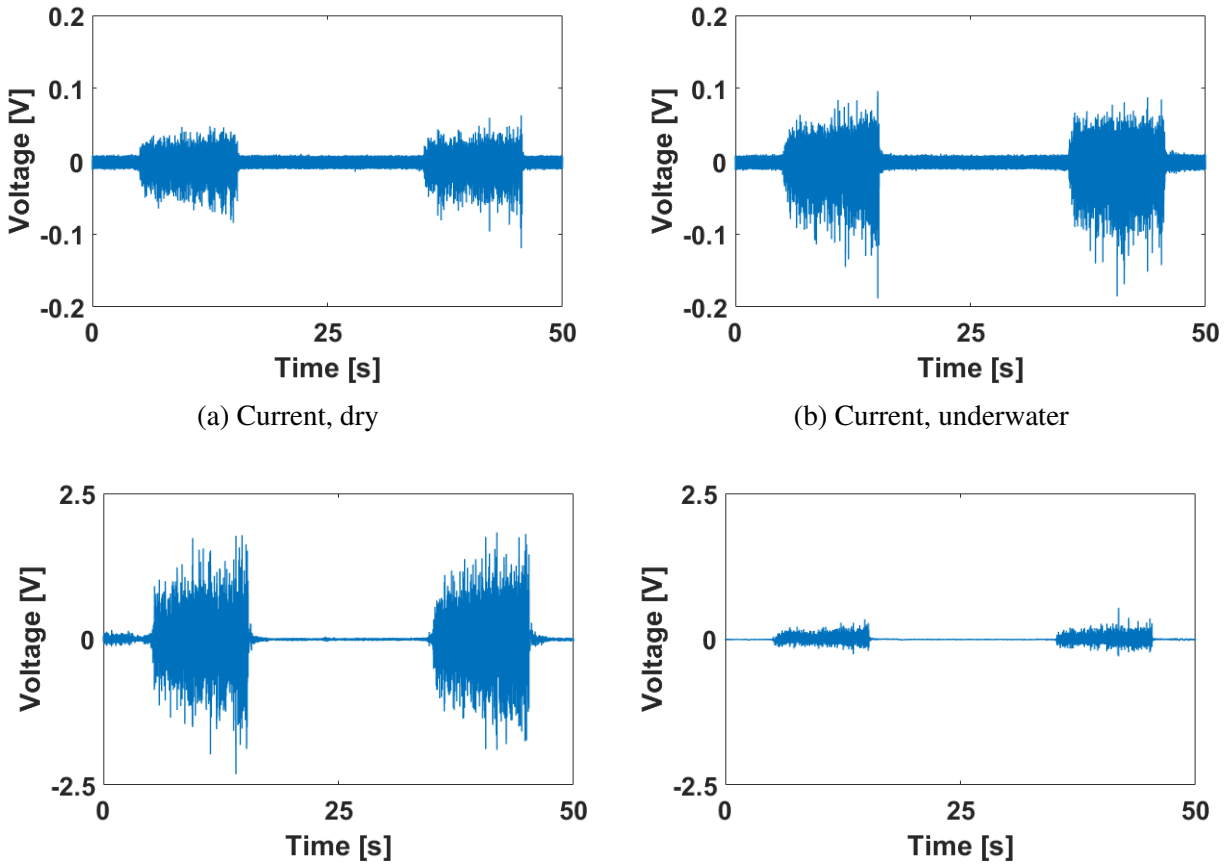

(a) Current, dry

(b) Current, underwater

(c) Potential, dry

(d) Potential, underwater

Figure 3.9: EMG raw data for subject 3 in all four conditions.

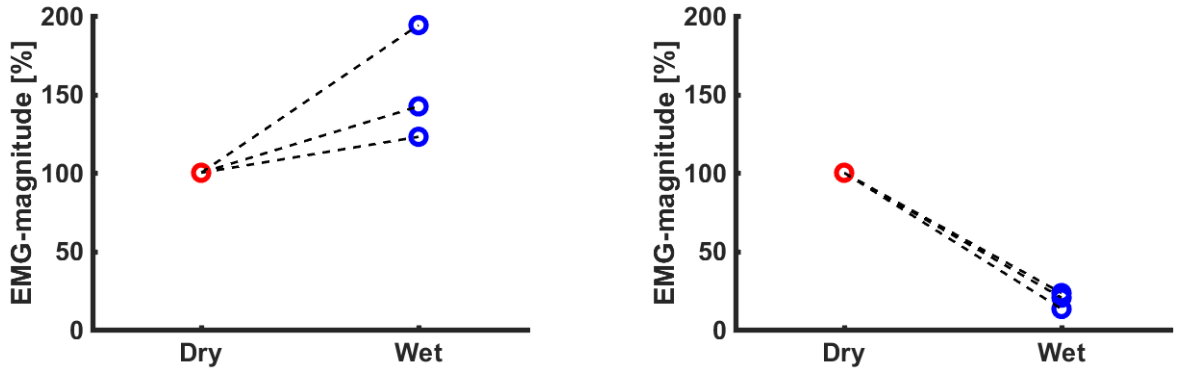

(a) Current

(b) Potential

Figure 3.10: Change of EMG-magnitude between conditions for current (a) and potential (b) amplifier. One point refers to the average EMG-magnitude from two trials for each of the three subjects. The EMG-magnitude was normalized to the respective value for the dry condition for each subject with each amplifier.

3.6.3 Discussion

The goal of this pilot study was to investigate the assumption that EMG-current signals measured with the new bipolar current amplifier would not show a reduction of signal amplitude. The raw signals subject 3 presented in Fig. 3.9 actually show an increased signal amplitude for the current measurement under water when compared to the dry condition. According to Table 3.2 subject 3 shows the highest increase among all subjects. For subject 1 and subject 2 there was a higher signal magnitude for the underwater condition than for the dry condition as well. This was also reported in underwater EMG measurements in [Whi14] and underwater ECG measurements in [Lau16]. The authors suggested that the liquid environment was beneficial for the electrode contact or caused an increased recording area on the skin.

In the results of the measurements with the potential amplifiers in Fig. 3.9c and Fig. 3.9d at first the higher signal amplitude for the dry condition compared to the current amplifier (Fig. 3.9a) becomes obvious. However, this difference is only due to the different ranges of output values of the two amplifier systems. The potential amplifier showed an amplitude range of ± 4 V, whereas the current amplifier system put out values in the range of ± 1 V.

Comparing the signals for dry and underwater condition, the potential amplifier shows a clear reduction of the amplitude (Fig. 3.9d). This behavior was consistently observed for all three subjects (Table 3.2 and Fig. 3.10). For EMG-potential measurements it has been reported before that the signal amplitude is drastically reduced in presence of water [Rai04, DSC10] or sweat [AE12]. Von Tscharner et al. [vT13] explained this phenomenon by intra-electrode cross talk between the two measurement points of the bipolar electrode.

3.6.4 Conclusion

Summing up the results from the evaluation study, the bipolar current amplifier showed promising results for measurements under water. It is therefore a suitable tool for studies in which subjects are sweating or performing movement tasks under water. The rejection of inter-electrode cross talk would also offer the possibility of using electrodes with a closer inter-electrode distance for the measurement of a more accurate differential of the MUAP.

3.7 Limitations

One drawback of the presented system was that the available isolation module for the moment only allowed the measurement of EMG signals from at most two muscles at a time. As in the running study, that was supposed to follow the hardware development, only signals from VM and VL should be collected, this was not a problem in the present project. Furthermore, the system required six 9 V batteries as power supplies as described in [CM16]. These batteries needed to be carried by the subjects during the following running study. In the backpack the subjects used during the running experiment the batteries were exposed to high impact forces. The shaking batteries were not ideal for the comfort of the subjects and furthermore the arising forces could cause problems for the sustainability of the battery connectors. The influence of the moving batteries could be minimized by attaching them tightly to the isolation module with tape and wrapping the whole device in cushioning material.

3.8 Summary of hardware development

In this chapter the development of the new bipolar EMG-current amplifier was described. The new system was designed to be compatible with a previously developed monopolar current amplifier. Simulations, test measurements and a pilot study with underwater measurements proofed that the amplifier performed in the expected way. The CMRR and the results of the underwater measurements point out the advantages of the bipolar current amplifier. The resistance against noise, motion artifacts, and humid environment were necessary features for an EMG signal acquisition device that was supposed to be used in a running study.

Chapter 4

Coherence and pattern analysis of running data

In order to investigate the hypotheses phrased in Chapter 1, a running study was conducted. The following sections give information about the methodology, the results will be presented and discussed.

4.1 Methods

The materials, the group of subjects, the study protocol, and the signal processing steps for the analysis of the running study will be presented in the following sections.

4.1.1 Materials

EMG signals were measured consecutively with the current amplifiers described in Chapter 3 and with standard bipolar potential amplifiers (Biovision, Wehrheim, Germany). Bipolar Ag/AgCl electrodes with a diameter of 10 mm and inter-electrode distance of 22 mm (Norotrode 20, Myotronics, Kent, WA, USA) were used for the EMG measurements. The acceleration of the runners' right foot was measured using single-axis accelerometers (ADXL 78, Analog Devices, Norwood, MA, USA). The analog EMG and accelerometer data was digitized by an 8-channel data acquisition card (Biovision, Wehrheim, Germany) and transferred to a standard laptop computer via USB connection. Custom written Matlab (Mathworks Inc., Natick, MA, USA) software was used for data recording. Subjects were running on an exercise treadmill (Quinton Q55, Mortara Instrument Inc., Milwaukee, WI, USA) and they wore a light weight, tightly fitting

running backpack (Ultimate Direction, Boulder, CO, USA) for carrying the necessary parts of the hardware. All subjects wore their own running shoes during the experiments.

4.1.2 Subjects

The group of subjects consisted of sixteen male individuals aged between 21 and 44 years. Basic anthropometric information is given in Table 4.1.

Table 4.1: Basic anthropometric information about the group of subjects

Characteristic	**Mean $\pm$ STD**
Age [years]	28 ± 5
Body height [cm]	176 ± 7
Body weight [kg]	71 ± 6

All subjects were in healthy condition and recreational athletes who exercised at least three times a week. Eleven of the subjects reported to be recreational runners with a range of distances between 5 and 55 km per week. The other five subjects performed other physical activities than running on a regular basis. An overview about the subjects and their running experience in terms of km per week is given in Table 4.2.

Table 4.2: Running experience (km / week) of the subjects

Subject	1	2	3	4	5	6	7	8	9	10	11	12	13	14	15	16
km / week	10	6	25	0	0	0	20	0	15	11	55	20	20	10	5	0

4.1.3 Study protocol

Preparations

EMG signals were measured from VM and VL of the right leg. In order to ensure high signal conductivity, the skin surface of the subjects was shaved, slightly abraded with sand paper and cleaned with alcohol wipes in the area around the electrode positions [Kon06]. Bipolar Ag/AgCl electrodes were placed over the muscle bellies of VM and VL. The respective locations and orientations were determined according to SENIAM guidelines for electrode placement and alignment [Her99].

As described in [CM16] the isolation module of the current amplifier system required a separate ground electrode for each amplifier. EMG signals from two muscles were measured,

therefore one ground electrode each was placed on the anterior superior iliac spine (ASIS) and on the tibial tuberosity. Fig. 4.1a shows a schematic of the electrode placement and measurement setup for the current measurements. For the potential amplifier, only the ground electrode at the ASIS was needed.

One objective of the study was to compare the result of the further analyses using EMG current and potential signals. Hence, every subject performed the following running protocol two times, once with each amplifier system. Therefore, extension cables were connected to the electrodes such that the amplifiers could be switched without touching or changing the electrodes and avoid a change in the electrode-skin contact. The respective amplifiers were connected to those extension cables. In case of the potential measurements the amplifiers were connected to the data acquisition card directly. For the current measurements, the amplifiers were connected to the isolation module (Section 3.2) and the isolation module was connected to the data acquisition card. The data acquisition card itself was connected to the laptop via USB. The subjects were asked to perform several contractions of VM and VL before the actual experiment to verify an adequate signal quality. The signal amplitude was visually inspected and in case of a too low or too high signal, the amplification was adjusted using the gain switch of the respective amplifier. The amplifiers, cables, and electrodes were tightly attached to the thigh using tape and an elastic bandage to make sure all connections were secured during the running study (Fig. 4.1c).

For the later analysis, the single running steps should be separated. For measurements of the reference point for the foot strike, two accelerometers were placed on the subject's right running shoe. One accelerometer was attached to the heel counter (in the following called *heel accelerometer*) and one to the lateral side of the midsole in the area of the head of the fifth metatarsal bone (in the following called *toe accelerometer*) as shown in Fig. 4.1b. The two accelerometers were connected to the same data acquisition card as the EMG amplifiers.

The data acquisition card and in case of the current amplifiers also the isolation module with the required 9 V batteries (Section 3.7) were placed in the backpack as shown in Fig. 4.1d. An appropriate amount of slack cable at all sensors and amplifiers was provided to not affect the subjects' comfort and range of motion during running.

Experimental procedure

All participants performed two trials of treadmill running, one for each of the two amplifier setups. The order of the amplifier setups was randomized over subjects in a balanced manner. Prior to the actual measurement a five minutes warm-up phase was performed. In this phase the speed of the treadmill was gradually increased to 6 mph (9.66 km/h, 2.68 m/s). The goal of the warm-up

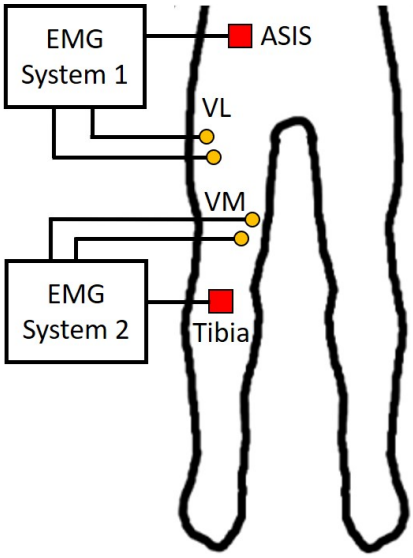

(a)

(b)

(c)

(d)

Figure 4.1: (a) Schematic of the electrode placement and measurement setup for the current measurements with two separate ground electrodes. (b) Placement of the accelerometers on the heel counter and in the area of the head of the fifth metatarsal bone. (c) Setup for measurements with current amplifiers on the subject. The ground electrode on the ASIS is not shown in this picture. (d) Setup of the running backpack with the data acquisition card attached to the straps and the isolation module placed in the lower compartment.

was to let the subjects familiarize with the measurement equipment and to make sure all sensors and amplifiers provided good signal quality. Furthermore, the warm-up should guarantee similar preconditions for both running trials, as the subject would always be already warmed-up and sweating prior to their second trial. After the warm-up the treadmill was set to the target speed of 6.5 mph (10.46 km/h, 2.91 m/s). This speed was chosen as it was supposed to allow recreational runners to perform steady state running over the required time of the study [Bar15]. After the treadmill had reached the target speed the data acquisition was started and the subjects ran for 15 minutes. EMG as well as acceleration data was collected with a sampling rate of $f_s = 2400\,\text{Hz}$ using custom built data acquisition software. Right after the first running trial the treadmill was stopped and the subjects were equipped with the second amplifier system after the amplifiers of the first system had been removed. Besides a gradual acceleration of the treadmill to the target speed there was no specific warm-up prior to the second running period. Again, 15 minutes of running data were collected using the same sampling rate and software as before.

This experimental protocol led to one data set from every subject for each amplifier system. One data set contained signals from VM and VL, as well as the accelerometer data.

4.1.4 Signal processing

Coherence and pattern analysis was performed using custom written scripts and functions in Matlab 2016b (Mathworks Inc., Natick, MA, USA). In the following, the processing algorithms are described in detail.

Step detection

As the running movement only requires muscle activation in the quadriceps muscles between late swing phase and midstance [Nov98], it was reasonable to cut out EMG signals that were within these points in time. The step detection algorithm determined those parts in the EMG signals that were then used for later analysis steps.

The accelerometers provided the necessary information for the step detection. From a visual inspection of the subjects' foot acceleration data, the subjects were assigned to the groups of rearfoot or forefoot strikers. A forefoot striker was identified if the peak acceleration related to the foot strike happened earlier in the toe-accelerometer than in the sensor at the heel and vice versa for rearfoot strikers. Examples for both rearfoot and forefoot strikers are presented in Fig. 4.2.

After this decision only the data from the respective accelerometer was used to determine the single steps. The single foot strike events were detected in a two-stage process. In the first stage

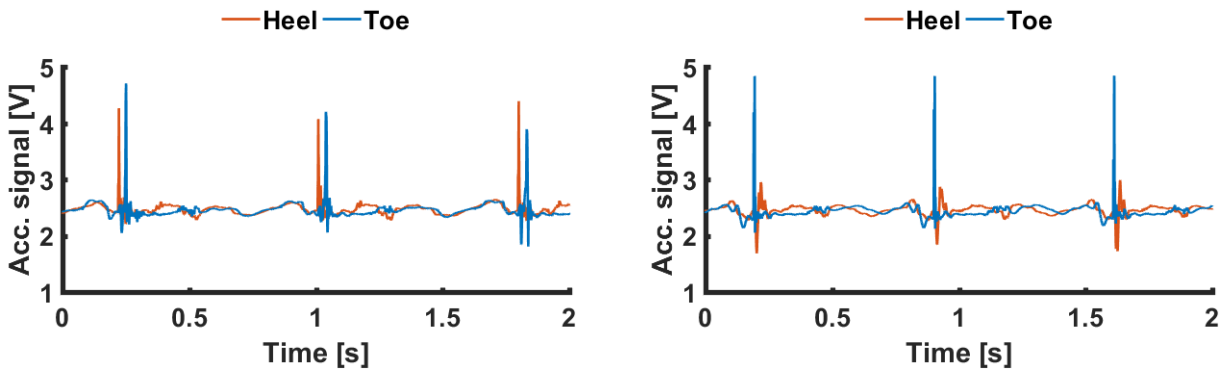

(a) (b)

Figure 4.2: Examples for data collected by the accelerometers attached to the heel (red) and at the toe area (blue) of the running shoe. (a) Data from a rearfoot striker, showing the peak in the heel accelerometer signal first. (b) Data from a forefoot striker, showing the peak in the toe accelerometer first.

the single steps were identified by applying a peak detection algorithm to the accelerometer signal of the whole running trial. In this stage a characteristic peak related to the foot strike was detected for every step in the data set. Due to individual differences in the running patterns of the subjects a second stage was applied for the exact determination of the reference point for the foot strike. The individual differences showed up in additional peaks in the accelerometer signals that could be falsely detected as the respective foot strike event. For the second stage signal windows of 200 ms before and after the detected peaks of stage one were created. The goal of the second stage was now to find the first characteristic peak within each window. An example for a correction is shown in Fig. 4.3: The first and the third peak in Fig. 4.3a were detected falsely by the first stage and were then corrected by the second stage resulting in the peak selection presented in Fig. 4.3b. The second stage was again based on an automatic peak detection. If this automatic selection failed, the respective foot strikes were determined manually after visual inspection. At the end of the step detection a vector containing the points in time for all foot strikes of the respective trial was returned and saved for the later processing steps.

EMG preprocessing

Several preprocessing steps were applied to the EMG raw data. The signals were converted from Volts to Millivolts using a simple multiplication by 1000 in order to have a higher magnitude of numerical values for the further analyses steps. The mean was subtracted to remove a possible offset in the signal. Finally, a custom notch filter that was optimized for the application to EMG

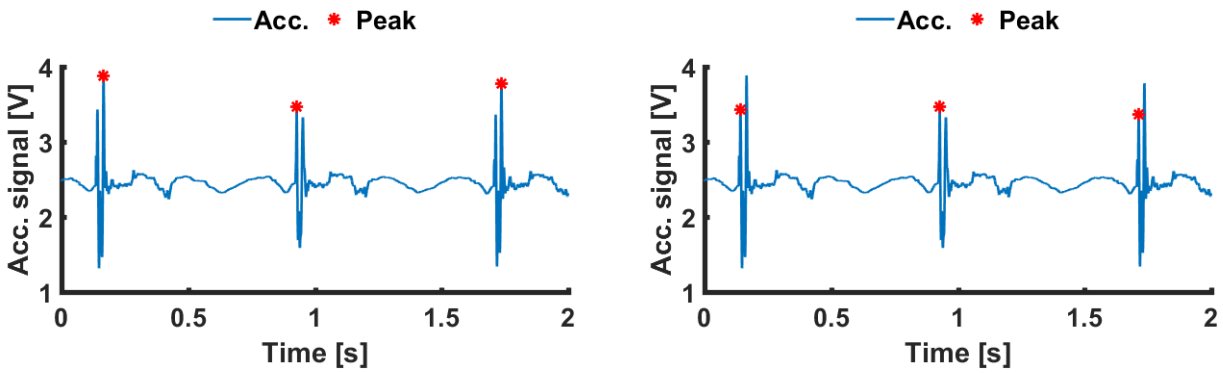

Figure 4.3: Example for the effect of the two stages of the step detection algorithm: (a) The first and the third peak in were detected falsely in the first stage. (b) After the second stage the two peaks are corrected.

signals was used to remove 60 Hz line frequency contamination. The preprocessed signals were then passed to the further processing pipeline.

Coherence analysis

In this study coherence was used as a measure of synchronization for the EMG signals from VM and VL during running as it was used before in different studies of intermuscular synchronization during squats or isometric contractions [Moh15, vT13].

The coherence analysis was applied to the raw EMG data of VM and VL from each subject separately for both of the two amplifier systems. For that purpose, the previously detected locations of the foot strikes were used to define windows of the EMG signals that were related to muscle activation. The windows had a size of 80 ms (192 data points) and contained EMG data from 30 ms (72 data points) before heel strike to 50 ms (120 data points) after heel strike. These parameters were defined after visual inspection of signals from all subjects. The goal was to define a window that was applicable for all subjects and all running steps. An example for the raw signals and the windows for the signal selection is shown in Fig. 4.4. The data from all these windows – as many windows as steps in the respective running trial – were extracted and for each window a zero padding was applied to reach a signal length of 256 samples.

The further coherence analysis was performed similar to [Moh15] and [Nan14]. Sequences of 30 consecutive running step windows were formed, where each sequence θ had a length of $30 \cdot 256 = 7680$ data points. The FFT was used to compute Fourier spectra $F_{VM_n}(\lambda)$ and $F_{VL_n}(\lambda)$ for each window n for the signals from VM and VL. For each sequence θ containing 30 windows

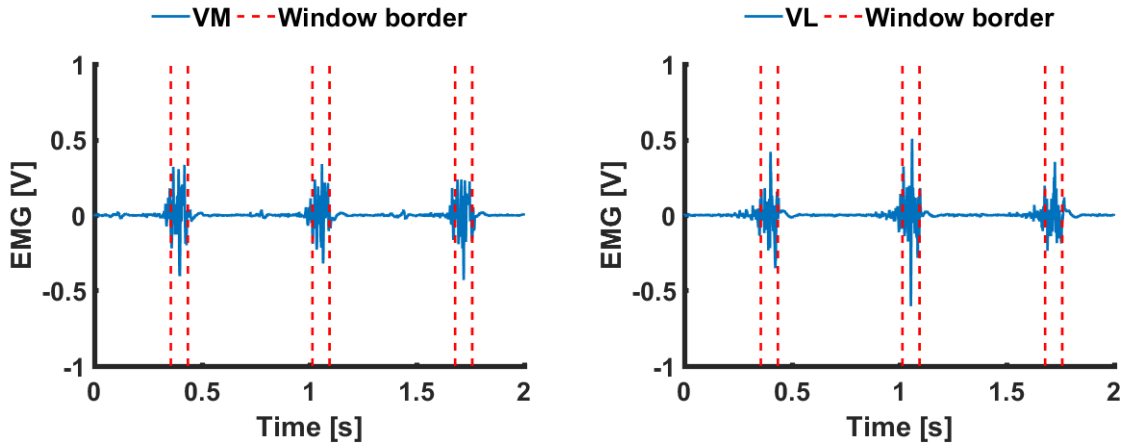

(a) (b)

Figure 4.4: EMG raw signals from (a) VM and (b) VL from three running steps. The signals belonging to muscle activation are captured in the short windows between the red dashed lines and were used for the coherence analysis.

the coherence spectrum was computed as a function of the frequency λ using the average cross-spectra normalized by the corresponding average auto-spectra across all windows n within the sequence. The formula for coherence is given as follows [Ros89]:

$$\mathrm{coh}_\theta(\lambda) = \frac{|\overline{F_{VM_n}(\lambda) \cdot F_{VL_n}(\lambda)^*}|^2}{\overline{(F_{VM_n}(\lambda) \cdot F_{VM_n}(\lambda)^*)} \cdot \overline{(F_{VL_n}(\lambda) \cdot F_{VL_n}(\lambda)^*)}} \tag{4.1}$$

where * indicates the conjugate complex value. As the coherence was computed for each frequency λ the computation resulted in a coherence spectrum. According to the length of a single (zero-padded) window and the sampling rate of 2400 Hz, the frequency resolution for both, the Fourier and the coherence spectra, was 9.375 Hz. The frequency range of interest was set from 5 to 258 Hz. Finally, the mean coherence spectrum over all sequences within one running trial was computed.

According to [Moh15], the significance of the computed coherence spectra can be evaluated using a reference coherence. Therefore, the EMG signal of the VL was shifted by one running step window with respect to the VM. The reference coherence was then computed for the VM and the shifted VL signal as described before. Fig. 4.5 shows an example for the coherence spectrum and the reference coherence measured from one subject in one running trial.

To reduce the result of the coherence analysis for each trial to one single value, the average coherence over frequencies was computed. This was done for the frequency range below 60 Hz and for the range of 60 to 250 Hz as relevant coherence values were observed in these separate

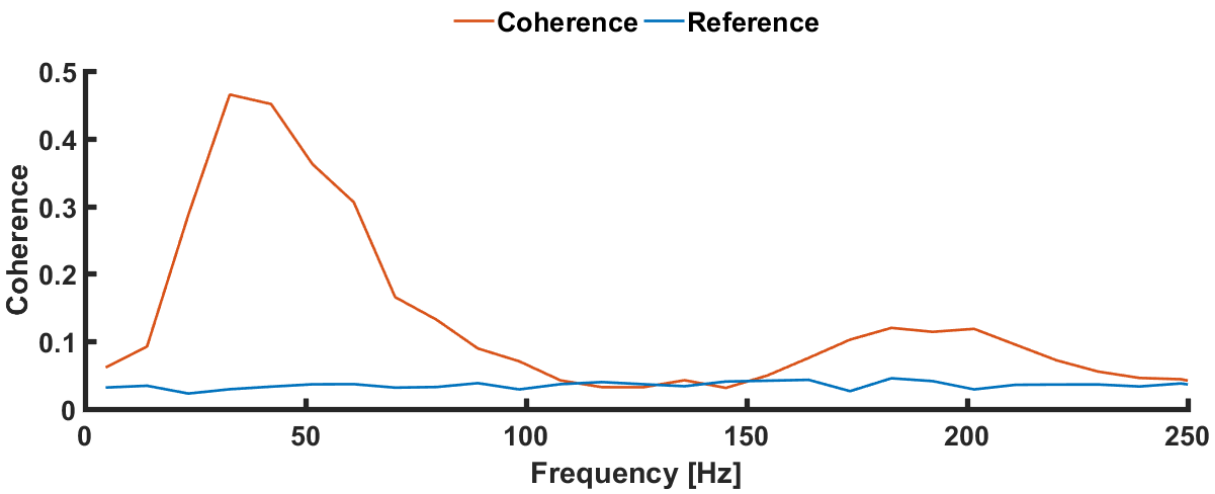

Figure 4.5: Mean coherence spectrum of EMG-currents from the vasti muscles measured during one running trial (red line). The blue line represents the significance boarder indicating the coherence between non-coherent signals. The figure is showing the average coherence spectrum over 37 blocks containing the data from 30 steps each.

bands. The average over the two frequency bands was also computed for the reference coherence.

Wavelet transform

For the pattern analysis of EMG signals regarding the task to look for clusters of muscle activation patterns during running within one muscle, the EMG signals were transformed to time-frequency space. The following parts of the analysis were executed separately for the data sets of all available conditions. One condition is defined as a combination of the following parameters:

1. Subject: index
2. Muscle: VM or VL
3. Amplifier system: current or potential

The data set for one condition is consisting of the data from either VM or VL from one single subject measured with one of the two amplifier systems.

Similar to the approach for the coherence analysis the previously detected locations of the foot strikes were used to define windows containing EMG signals of interest. The windows for this part of the analysis had an original size of 400 ms (960 data points) and were placed symmetrically around the respective time points of the foot strikes. According to the usual stance time at the chosen running speed of 6.5 mph [Mun87] and the fact that the quadriceps muscles are active in

the late swing and the early stance phase [Nov98], the chosen window size was sufficiently large to capture all relevant EMG data related to the running movement.

The data from all windows – as many windows as steps in the respective running trial – were extracted and passed to a time frequency analysis using non-linearly scaled wavelets as presented in [vT00]. Each wavelet ψ was defined in frequency space as a function of frequency f, center frequency cf and $scale$:

$$\psi(f, cf, scale) := \left(\frac{f}{cf}\right)^{cf \cdot scale} \cdot \mathrm{e}^{\left(\frac{-f}{cf}+1\right) \cdot cf \cdot scale} \tag{4.2}$$

The center frequency shows the position of the maximum of the wavelet in frequency space. A set of wavelets was created using several center frequencies indexed by $j = 0$ to J. The calculation of the center frequencies was performed as follows:

$$cf_j := \frac{1}{scale} \cdot (j + q)^r \tag{4.3}$$

Similar as in [vT00] the parameter q was set to 1.45 and r was set to 1.959. The original scale of 0.3 in [vT00] was changed to 1.5 and a number of J = 20 wavelets were computed. This adaption was necessary to achieve a higher frequency resolution in the low frequencies of interest between 2.5 and 250 Hz. The center frequencies are listed in Table 4.3 and the respective wavelets in frequency space are presented in Fig. 4.6a. Two examples of the wavelets, number 5 and 15, are also shown in time domain in Fig. 4.6b.

The wavelet transform for one window was calculated by filtering the EMG signal with each of the 20 wavelets [vT09]. The EMG signal was transformed to Fourier space using a FFT and

Table 4.3: Center frequencies cf of the wavelets indexed by j

Wavelet j	**Center Freq. [Hz]**	**Wavelet j**	**Center Freq. [Hz]**
1	2.5	11	80.0
2	5.0	12	92.5
3	7.5	13	107.5
4	12.5	14	125.0
5	17.5	15	142.5
6	25.0	16	160.0
7	35.0	17	180.0
8	42.5	18	202.5
9	55.0	19	222.5
10	65.0	20	247.5

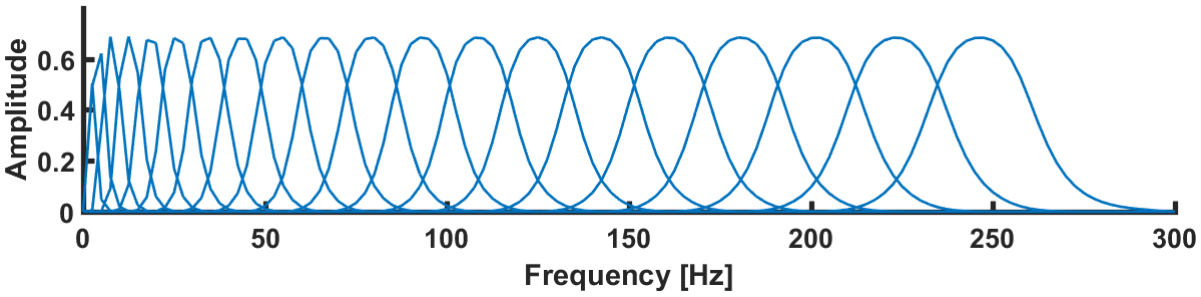

(a)

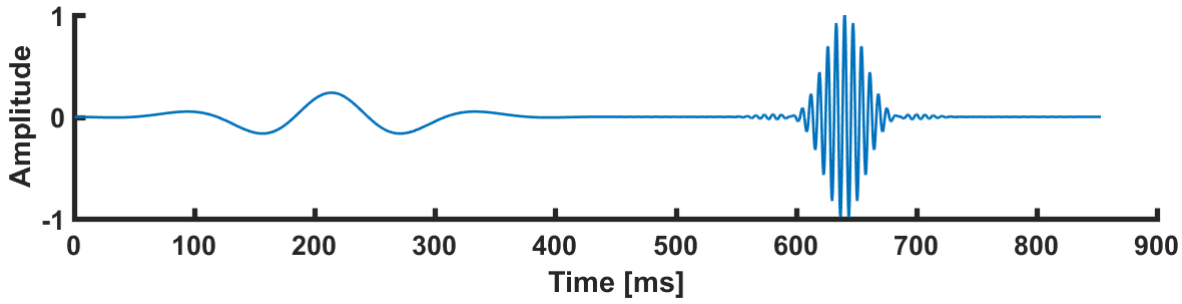

(b)

Figure 4.6: (a) Filter-bank of 20 wavelets in frequency space. (b) Wavelet 5 and 15 in time domain. Obviously, the higher order wavelet shows more oscillations with a higher frequency.

the filtering was then performed as a multiplication in frequency space. The resulting 20 filtered signals per window were reconstructed to time domain using the inverse FFT. The intensity $p_{j,n}$ of the EMG signal for the frequency band covered by wavelet j at each time point t_n was computed as the square root the power of the wavelet transformed EMG signal. The result of the wavelet transform for one window was a wavelet intensity pattern (WIP) with time and frequency domain that is displayed as a contour plot (Fig. 4.7a). In this plot the time domain is represented on the horizontal axis and the vertical axis shows center frequencies. The intensity values $p_{j,n}$ are indicated in color coding.

The goal for the later analysis was to use all WIPs of one running trial for machine learning methods where the WIPs would be used as vectors spanning a vector space called pattern space [vT09]. A common problem in machine learning is the curse of dimensionality [Dud12, Bis06]. The resulting WIP of the wavelet transform for one step was a matrix from $\mathbb{R}^{20\times960}$ (20 wavelets and 960 time points) with 19200 entries or dimensions. The goal, however, was to gain a dimensionality that is lower than the number of running steps within one trial to have a well-defined pattern space.

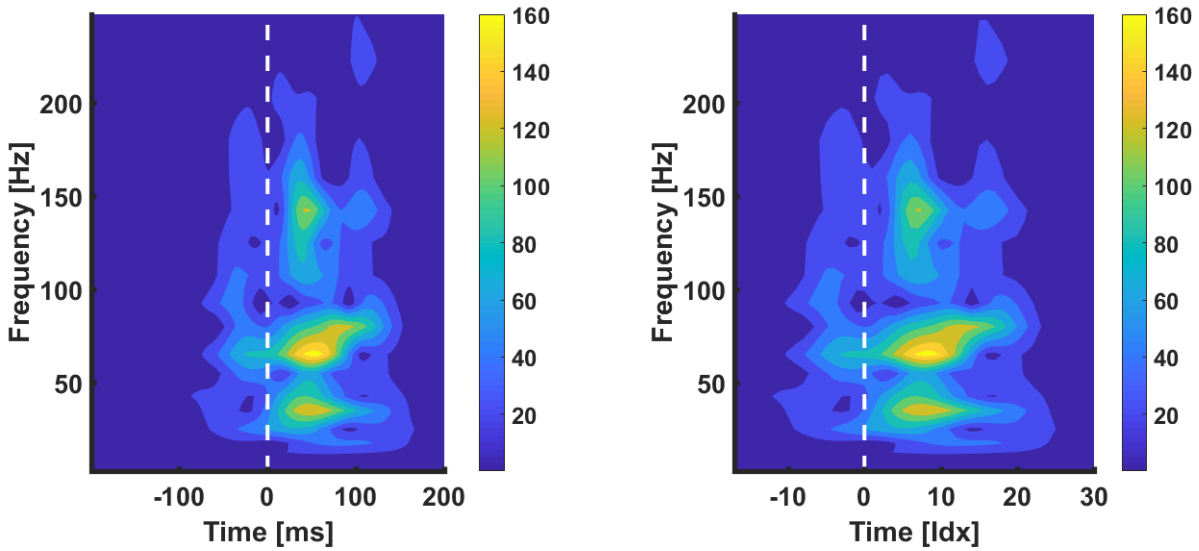

(a) (b)

Figure 4.7: Example of the wavelet intensity pattern (WIP) from one running step measured from VM with the current amplifier. The intensity values $p_{j,n}$ are indicated in color coding. The time of the foot strike is shown as a white dashed line. (a) shows the data in the original time scaling with $960 \cdot 20$ values. (b) shows the pattern after cutting away the first 80 ms in time domain and resampling the remaining data down to 48 samples in time domain.

Therefore, two further processing steps were applied:

1. By visual inspection it became obvious that the very left area of the WIPs, which shows the data early before the foot strike, did not show any relevant information in terms of muscle activation. Hence the first 20 % of the data in time domain (80 ms or 192 data points) were removed. After this measure the time axis of the WIPs was asymmetric. The time point of the foot strike was not in the middle of the time axis anymore but divided the time axis in the ratio 3:5 (Fig. 4.7b).

2. After cutting out the first 192 samples in time domain, the resulting matrix for one WIP had a dimensionality of $\mathbb{R}^{20\times768}$. By interpolating 16 original time samples to 1 new sample the dimensionality was further reduced to $\mathbb{R}^{20\times48}$ which equals to 960 dimensions.

As subjects would perform at least 1000 steps per trial in the running study, this was an appropriate reduction of dimensionality. There was no reduction in frequency domain to keep the high resolution in the frequency range of interest.

Wavelet spectrum

An approximation of the power spectral density of each pattern is obtained by summing up the intensity values over time:

$$P(j) = \sum_{n=1}^{48} p_{j,n} \qquad j = 1, ..., 20 \tag{4.4}$$

After eliminating the time information, only the frequency information of the WIP is left, one value for each of the 20 center frequencies. This frequency spectrum for each step was defined as wavelet spectrum and the average wavelet spectrum $\overline{P(j)}$ over all steps of one running trial was calculated. A normalization factor c_{norm} was computed by summing up the average wavelet spectrum values related to center frequencies above 107.5 Hz. The modulation of the EMG signal caused by motor unit clustering is only affecting the low frequency bands below 100 Hz. Hence, the high frequencies offer a valid band for a normalization factor. According to the center frequencies listed in Table 4.3 the normalization factor was computed as follows:

$$c_{norm} = \sum_{j=13}^{20} \overline{P(j)} \tag{4.5}$$

Afterwards each of the intensity values $p_{j,n}$ in all steps of the respective trial was divided by the normalization factor and multiplied by 1000 to keep a higher range of numerical values in the patterns.

Finally, for a comparison of the overall result for potential and current amplifier signals the average wavelet spectra over all measurements with current and potential amplifiers were computed. This calculation resulted in four spectra for the four conditions based on the two amplifier systems and the two muscles that were investigated.

Data reorganization

The normalized WIPs of one whole running trial were now available in a three-dimensional matrix $\mathbb{R}^{20\times48\times S}$, where S is the number of steps available for the respective trial. It was previously mentioned that in the later analysis all WIPs from one running trial should be used as vectors spanning a vector space. Therefore, it was necessary to reorganize the data such that the intensity pattern of each step was available as a column vector. The values from a single WIP were read in line by line and transformed to a column vector d_s, where s is the step index, with the resulting dimensionality of $\mathbb{R}^{960\times1}$. This operation was done for all WIPs of one trial to form a large measurement matrix $D \in \mathbb{R}^{960\times S}$, where again S represents the number of steps in the respective trial. A separate matrix D was produced for all available conditions, meaning one matrix D for the data from VM or VL from one subject using one of the two amplifier systems.

Principal component analysis

Principal component analysis (PCA) is a common technique that yields a coordinate transform to a new orthonormal base and is applied for dimensionality reduction [vT09, Bis06]. Given from the previously described processing stages was one data matrix D for each condition, where each column vector d_s of D contained the WIP for the running step indexed by s. Each vector d_s had a dimensionality of M, where M = 960 as described in the previous section.

The goal of the PCA was to project the data set D onto a new vector space having a dimensionality $m < M$ while maximizing the variance of the projected data. The space providing the maximized spread of the data is spanned by the eigenvectors of the covariance matrix of D [Bis06]. Each eigenvector can again be displayed as a WIP and is thus called a principal pattern (PP) of D [vT09]. The eigenvectors / PPs and their corresponding eigenvalues were computed using a singular value decomposition (SVD) and stored in a matrix $V \in \mathbb{R}^{960\times960}$, where each row vector of V contained one PP. Each of the original d_s can be represented as a linear combination of the PPs in V. Each of the PPs contributes to this linear combination with a specific weight, such

that a weight vector w_s contains the weights needed for the reconstruction of a specific pattern d_s [vT09]. The weight matrix W containing the weights w_s for each step in D in columns was computed by

$$W = V \cdot D \tag{4.6}$$

and each intensity pattern d_s can be reconstructed by

$$d_s = V^T \cdot w_s \tag{4.7}$$

Additionally to the traditional PCA, the residual mean d_{res} was computed as a PP and added to the matrix V. Therefore, the mean pattern $\bar{d}$ from all patterns d_s and its weight vector $w_{\bar{d}}$ were computed:

$$w_{\bar{d}} = V \cdot \bar{d} \tag{4.8}$$

Using $w_{\bar{d}}$ the reconstruction of $\bar{d}$ was computed:

$$\bar{d}_{recon} = V^T \cdot w_{\bar{d}}; \tag{4.9}$$

The residual mean was defined as the difference between the original mean pattern $\bar{d}$ and the reconstructed mean pattern $\bar{d}_{recon}$

$$d_{res} = \bar{d} - \bar{d}_{recon} \tag{4.10}$$

and then normalized by its Euclidean norm. This vector can also be interpreted as a pattern. It is orthogonal to the pattern space defined by the PPs in V and is completing the space. Thus, the residual mean vector was inserted as the first row of V.

According to Eq. (4.6) and Eq. (4.7), the WIP d_s for each running step in the data set D is now represented by a weight vector w_s in W, where w_s contains the weights for the new base formed by the PPs in V. As previously mentioned, the goal of applying PCA was to reduce the dimensionality of the data set D. Therefore, the PPs in V were sorted in decreasing order of their corresponding eigenvalues [End14] with exception of the residual mean, which was always kept in the first row of V. The eigenvalues describe the variance that is explained by the corresponding PPs and can be expressed as a percentage of the sum across all eigenvalues. For the purpose of dimensionality reduction only those PPs (or those rows in V) were kept, that belong to the eigenvalues describing 90 % of the total variance of the data. After this operation the PPs which mainly contribute noise to a reconstructed pattern were removed [vT09]. According to the elimination of PPs in V, also the respective rows in the weight matrix W were removed, resulting in reduced weight vectors w_s with a dimensionality of $\mathbb{R}^{m\times 1}$ where m is the number of PPs that

were kept. Thus, m is describing the resulting dimensionality after applying PCA and it applies that $m < M$.

Clustering

With respect to the second Hypothesis (Chapter 1) a method had to be found to investigate if a finite number of task-specific EMG signal patterns is present within one muscle. In terms of machine learning the task was to assign class labels to the data of the several running steps within one trial in such a way that those patterns that receive the same class label share some common properties. As in the case of the EMG signal patterns no preclassified, labeled instances were available, a method from the area of unsupervised classification or clustering needed to be considered. Clustering methods are able to find groups in the data set the way that samples from the same group are more similar to each other than samples belonging to different groups [Ban12, Bis06]. The clustering was applied to the output of the previously described PCA, which was the a weight matrix W resulting from the input data matrix D, where each column vector w_s described the data belonging to the WIP of the running step indexed by s.

For this thesis, agglomerative hierarchical clustering was chosen for the clustering task [Dud12, Ame06]. In this approach all S instances from a data set are first assigned to their own cluster D_i, where S is equal to the number of running steps contained in the data set of a single trial. In an iterative way the two nearest clusters D_i and D_j are identified and merged together to a new cluster. This iteration is performed until there is only one cluster left, containing all data samples that are grouped together in subclusters in a hierarchical manner.

Two different graphical representations of hierarchical clustering are presented in Fig. 4.8. As mentioned before in every iteration of the clustering algorithm the two nearest clusters have to be found. To find two nearest clusters a similarity or distance measure had to be defined. In the case of the EMG intensity patterns several pilot experiments have identified that the correlation coefficient showed the most promising results as opposed to the classically used Euclidean distance. Therefore, the correlation coefficient for each possible pair of data samples, meaning for each possible pair of weight vectors w_s was computed. The correlation coefficient was defined as [Mat17a]

$$\rho(w_i, w_j) = \frac{cov(w_i, w_j)}{\sigma_{w_i}\sigma_{w_j}} \tag{4.11}$$

where $cov(w_i, w_j)$ is the covariance matrix of w_i and w_j, σ_{w_i} and σ_{w_j} are the standard deviations of the weight vectors w_i and w_j. The values for the correlation coefficient were stored in a matrix $R \in \mathbb{R}^{S\times S}$, S representing the number of patterns in the respective data set. Within R the

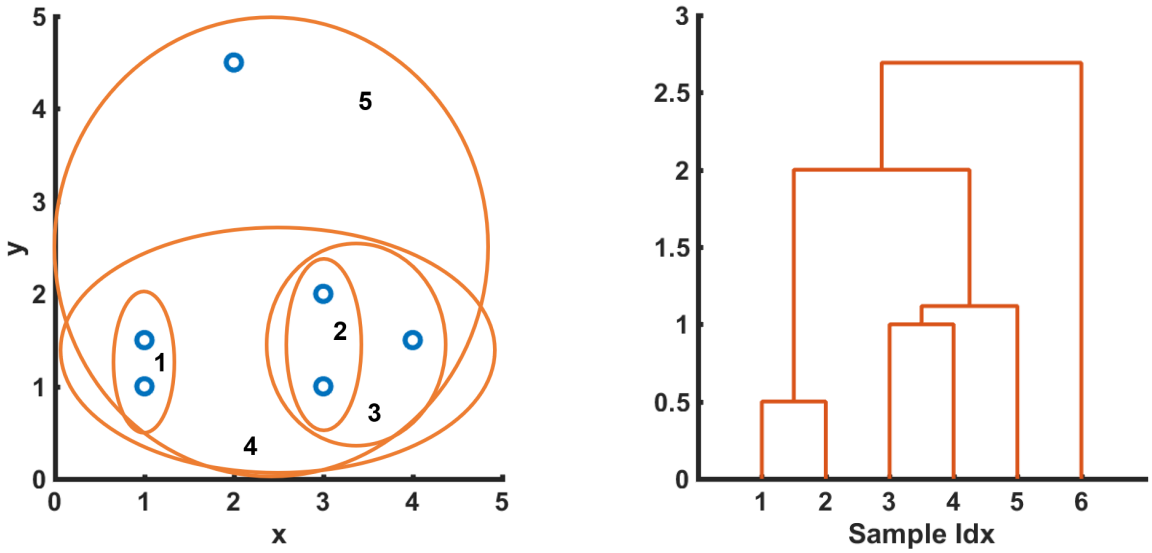

(a) (b)

Figure 4.8: Example for hierarchical clustering with six data points in two dimensions and in two graphical representations. (a) shows the set or Venn diagram representation of the data. It reveals the hierarchical structure but not the quantitative distances between clusters. The hierarchical levels of the clusters are numbered in black. (b) Shows the resulting dendrogram. The vertical axis represents a generalized measure of similarity among clusters (Euclidean distance in the example).

correlation coefficient $\rho(w_i, w_j)$ is stored at position (i, j). In addition, the corresponding matrix of p-values ranging from 0 to 1 was computed, where values close to 0 correspond to a significant correlation between the respective samples. In order to only keep those correlation coefficients between pairs w_i and w_j that show a significant correlation in a 95 % confidence interval, all values in R corresponding to p-values higher than 0.05 were set to 0.

As clustering methods usually use a distance between samples, the dissimilarity δ was defined as

$$\delta(w_i, w_j) = 1 - \rho(w_i, w_j). \tag{4.12}$$

The matrix containing the values $\delta(w_i, w_j)$ was reorganized such that it could be passed to the built in Matlab function `linkage`, which was capable of computing the agglomerative hierarchical clustering tree [Mat17b].

Besides the distance metric, the method for computing the distance between clusters had to be determined. In this thesis the `method`-parameter of the `linkage`-function was set to `complete`, yielding the complete-linkage algorithm [Mat17b, Dud12]. In the complete-linkage algorithm, also called the furthest distance algorithm, the distance between two clusters is defined by the most distant samples in the two clusters [Dud12]. In the case of the dissimilarity based on the correlation coefficient the furthest distance is referring to the least correlated samples in two clusters.

As described before, the hierarchical clustering was run the way that it would terminate when there is only one cluster left. In the case of this study there was no predefined number of clusters that was supposed to be found and it was also expected that the number of clusters was subject specific. Therefore, a threshold for the maximum dissimilarity of any two clusters was determined. If this threshold was passed two clusters D_i and D_j were not merged to a new cluster. The threshold was set to 0.2, corresponding to a correlation coefficient of 0.8, where according to [Tay90] a correlation coefficient of 0.8 represents a high correlation. Consequently, all signal patterns within each of the resulting clusters had to show a correlation of higher than 0.8.

Using the dissimilarity matrix based on correlation coefficients and the cutoff value of 0.2, the clustering was performed separately for the weight matrices W of each condition. As a result of the clustering for each condition the number of clusters was obtained. Furthermore, a histogram showing the distribution of the number of patterns assigned to the clusters was created, from which the median and the maximum number of patterns per cluster could be identified.

Surrogate signals

The significance of the clustering result based on the measured EMG data was evaluated in a comparison against artificial surrogate signals. If the measured EMG signals did not have certain repeatably appearing characteristics but were all random and different from each other, the clustering using artificially produced surrogate signals should yield similar results compared to the clustering of the real signals. The resulting number of clusters and the distribution of the number of patterns per cluster would be similar in this case.

Therefore, a set of surrogate signals was produced for each available condition in the following way: As described before the weight matrix W was computed from the WIPs of one trial using PCA. W contained the weight vectors w_s in its columns and each w_s represents the WIP for the step with index s in the new base defined by the PCA. It was now possible to calculate the mean weight vector $\bar{w} \in \mathbb{R}^{m \times 1}$ over all columns of W, where m is the dimensionality of the vector space after the PCA. Furthermore, the standard deviation σ_w of the weights in each row was computed, also resulting in a vector $\sigma_w \in \mathbb{R}^{m \times 1}$.

Using $\bar{w}$ and σ_w, normal distributions for each dimension were computed. To create surrogate signals, random samples from this normal distribution were drawn and stored in surrogate weight vectors $w_{s_{sur}} \in \mathbb{R}^{m \times 1}$. In this way a weight matrix $W_{sur} \in \mathbb{R}^{m \times S}$ was created, containing as many surrogate signals as there were running steps in the original data set. This approach allowed the generation of artificial signals that still showed the general structure of the original WIPs, however the fine structure was defined by a random combination of values.

The matrix W_{sur} was then passed to the same clustering algorithm described in the previous section. As the calculation of W_{sur} was based on a random sampling of normal distributions, the steps of generating W_{sur} and applying the clustering algorithm to it were repeated 25 times. The average clustering result was used for the comparison with the clustering based on the original data in W.

Statistical analysis

For the statistical analysis of the coherence results, 95 % confidence intervals of the resulting values were computed to determine differences between the average coherence and the average reference coherence in the two frequency bands described before. A significant difference was determined when the 95 % confidence intervals of the respective values did not overlap.

The results of the clustering using the real measured EMG data and the artificially produced surrogate signals were compared using the median number of steps per cluster. A significance of the difference between median values was determined using a Wilcoxon rank sum test.

4.2 Results

In the following sections the result of the running study will be presented. After an overview about the collected data, the results for coherence and clustering analysis are shown. In the two analysis sections typical results of individual subjects will be shown first to reveal general properties of EMG of the vasti muscles during running. These examples are followed by the overall result of the respective analysis for all subjects.

4.2.1 Data collection

In Section 4.1.3 it was described that 16 subjects took part in the study. Due to technical difficulties and poor signal quality in some of the measurements, data from 4 subjects needed to be excluded. The remaining subjects performed two running trials each, hence a complete data set of measurements from VM and VL with current and potential amplifiers could be acquired from 12 subjects. Altogether these subjects performed 29756 running steps. Examples for EMG raw data from current and potential amplifier and from VM and VL are shown in Fig. 4.9. The overall average wavelet spectra for the two amplifier systems calculated for the two muscles are presented in Fig. 4.10.

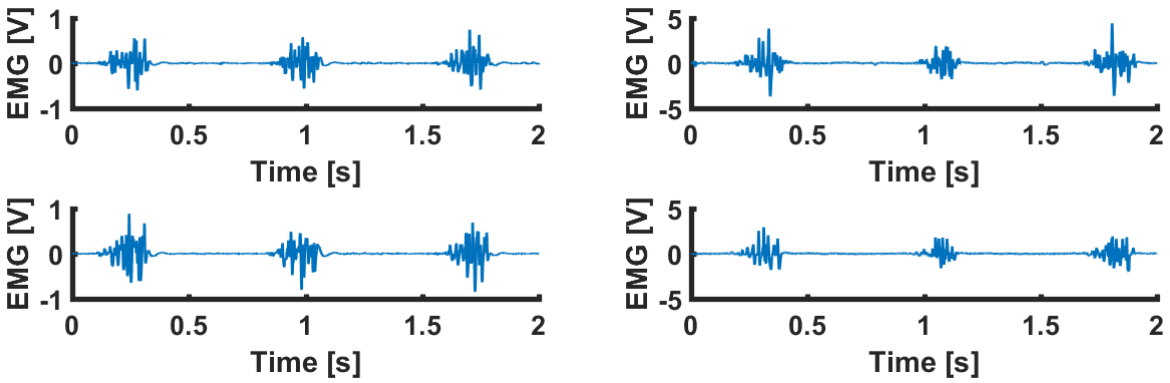

(a) Current

(b) Potential

Figure 4.9: Examples for data collected by the two EMG amplifier systems from subject 5: (a) Signals measured with current amplifiers. (b) Signals measured with potential amplifiers. The top row shows VM signals, bottom row shows VL signals.

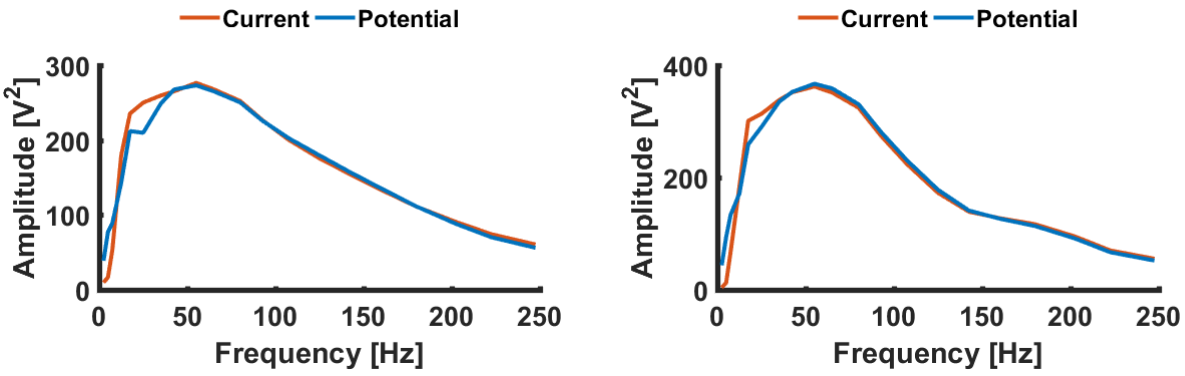

(a) (b)

Figure 4.10: Wavelet spectra over all steps from all 12 subjects for (a) VM and (b) VL.

4.2.2 Coherence analysis

Fig. 4.11 shows the coherence spectra of a single subject for the current and the potential measurements. The mean coherence spectra for all current and potential measurements are shown in Fig. 4.12. With respect to the mean spectra in Fig. 4.12, the example in Fig. 4.11 is representing a typical coherence result. There are frequency bands with a distinct significant coherence between 5 and 100 Hz, and between 160 and 200 Hz. The two frequency bands have center frequencies at about 30 Hz and 180 Hz, respectively. In terms of general shape, magnitude, and standard error, the coherence analysis with signals from the current and the potential amplifiers show a similar result in a single example (Fig. 4.11) as well as overall (Fig. 4.12). In Fig. 4.13 the average values of reference coherence and the actual coherence spectra in the two frequency bands of 5 to 60 Hz and 60 to 250 Hz are shown for current measurements and potential measurements. For all subjects the mean value for the coherence compared to the reference is significantly higher in the signals from both amplifier systems in both frequency bands ($p < 0.05$). The respective values to Fig. 4.13 are displayed in Table 4.4.

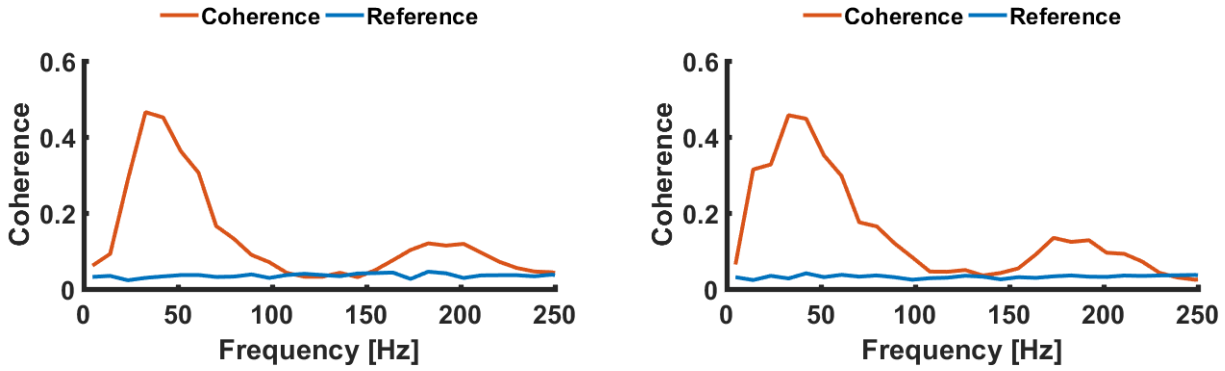

(a) (b)

Figure 4.11: Example coherence spectra (red line) computed with the data of the two EMG amplifier systems from subject 6: (a) Signals measured with current amplifiers. (b) Signals measured with potential amplifiers. The blue spectrum in both graphs shows the significance boarder indicating the coherence between shifted signals.

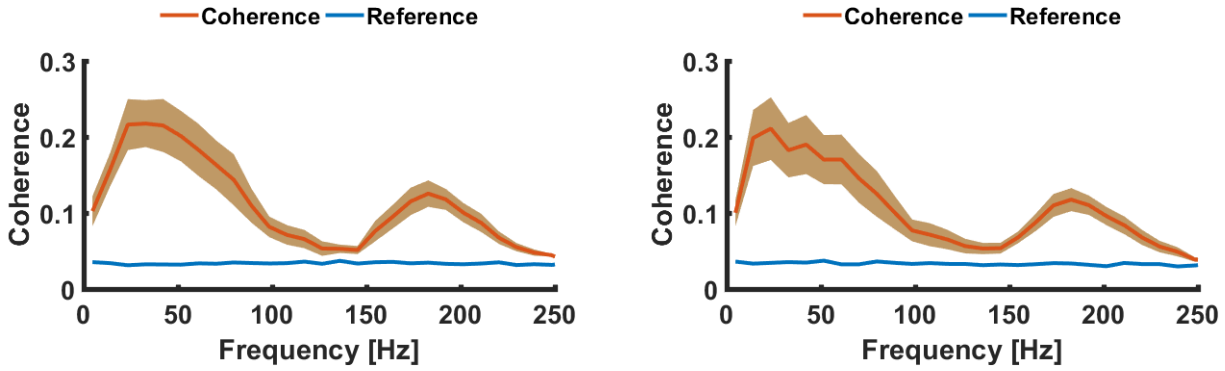

(a) (b)

Figure 4.12: Mean coherence spectra (red line) computed with the data of the two EMG amplifier systems from all subjects: (a) Signals measured with current amplifiers. (b) Signals measured with potential amplifiers. The blue spectrum in both graphs shows the significance boarder indicating the coherence between shifted signals. The shaded area is representing the standard error of the spectra.

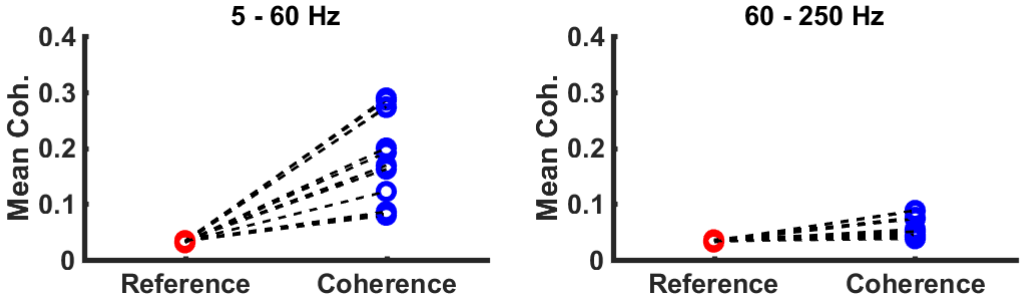

(a)

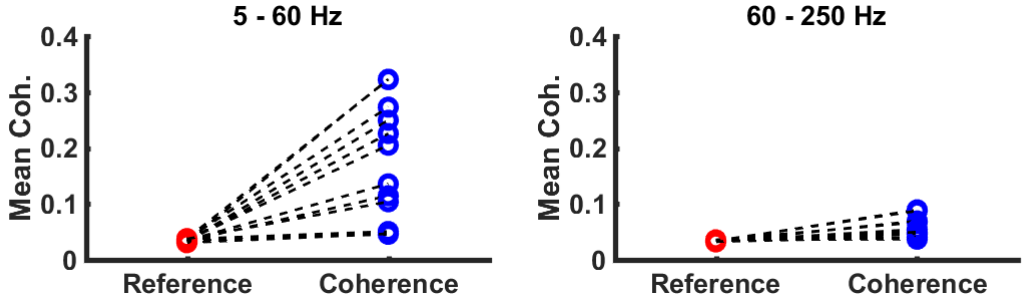

(b)

Figure 4.13: Average values of reference coherence and the actual coherence spectra in the two frequency bands for (a) current measurements and (b) potential measurements. For all subjects there is a significantly higher value for the coherence compared to the reference.

Table 4.4: Average values of reference coherence and the actual coherence spectra in the two frequency bands. The frequency band from 5 to 60 Hz is represented by the *60*, the band from 60 to 250 Hz by *250*, respectively. Values for current measurements are shown under *C*, for potentials under *P*.

Subject	Ref. 60 C	Avg. 60 C	Ref. 250 C	Avg. 250 C	Ref. 60 P	Avg. 60 P	Ref. 250 P	Avg. 250 P
1	0.0306	0.1922	0.0319	0.0503	0.0347	0.1359	0.0330	0.0465
2	0.0332	0.1689	0.0334	0.0550	0.0341	0.1147	0.0333	0.0491
3	0.0345	0.0830	0.0328	0.0408	0.0372	0.0508	0.0331	0.0406
4	0.0332	0.2724	0.0358	0.0759	0.0324	0.2496	0.0357	0.0671
5	0.0318	0.2000	0.0331	0.0736	0.0351	0.2050	0.0321	0.0696
6	0.0322	0.2894	0.0356	0.0527	0.0324	0.3230	0.0330	0.0547
7	0.0340	0.2855	0.0340	0.0870	0.0372	0.2730	0.0335	0.0895
8	0.0330	0.1223	0.0340	0.0378	0.0347	0.0457	0.0358	0.0370
9	0.0316	0.2737	0.0339	0.0884	0.0381	0.3221	0.0341	0.0876
10	0.0342	0.1622	0.0340	0.0427	0.0336	0.2258	0.0327	0.0406
11	0.0334	0.0797	0.0350	0.0448	0.0307	0.0468	0.0326	0.0470
12	0.0344	0.0861	0.0335	0.0506	0.0373	0.1039	0.0325	0.0497

4.2.3 Clustering

As described in Section 4.1.4 the clustering of the EMG signals from one single muscle was performed after the application of a wavelet transform and a PCA to the original signals. The mean WIPs over all steps for VM and VL for current and potential measurements for 2 subjects reveal subject specific results (Fig. 4.14 and Fig. 4.15). The mean WIPs for all subjects and all conditions are available in Appendix C. The original dimensionality of the WIPs was 960 and could on average be reduced to an about 20 times lower new dimensionality by the PCA. The WIPs of the first five PPs for subject 3 are shown together with the WIP of the residual mean in Fig. 4.16 for current and potential measurements. Over all four conditions, between 28 and 57 PPs were necessary to describe 90 % of the variance of the data (average: 41).

The clustering approach described in Section 4.1.4 resulted in dendrograms and histograms for VM and VL for each amplifier system. Examples of these graphs for the current measurement of subject 1 are shown in Fig. 4.17 and Fig. 4.18. One can compute the mean of all steps in the four biggest clusters of one measurement as shown in Fig. 4.19. The examples show that the different clusters are basically caused by the combined activity in different frequency bands that get activated individually in the WIPs of different clusters. Fig. 4.20 shows four WIPs from the same cluster and gives insight about the similarity of the WIPs that were assigned to the same cluster.

Finally, Table 4.5, Table 4.6, Table 4.7, and Table 4.8 provide an overview about the quantitative results of the clustering for all 12 subjects from whom EMG signals were measured from VM and VL with current and potential amplifiers. Over all four conditions, on average 69 clusters of WIPs were determined, where the average median number of steps assigned to one cluster was 19. For the surrogate signals on average 120 clusters were found, here the average median number of steps per cluster was 9. Based on the Wilcoxon rank sum test the median values for the real signals are significantly higher than those of the surrogate signals for all subjects in all four conditions. Hence, the WIPs of the real EMG signals were grouped into significantly larger clusters, whereas the random surrogate signals did not show sufficient structure to form big groups.

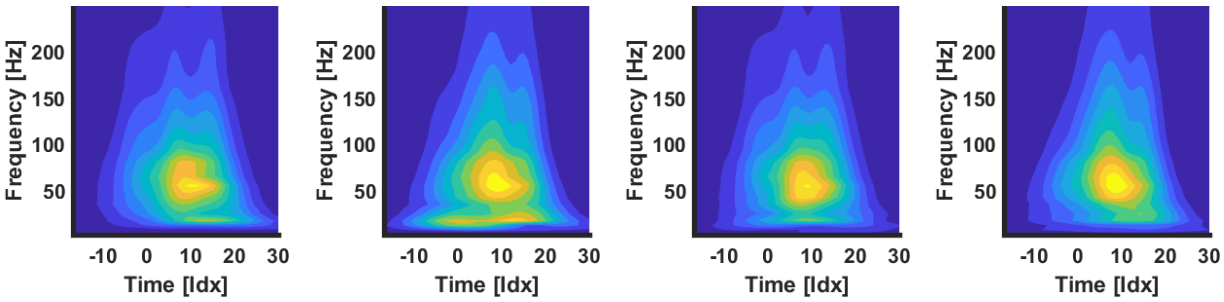

(a) (b) (c) (d)

Figure 4.14: Mean wavelet intensity patterns (WIP) for (a) VM current, (b) VL current, (c) VM potential, (d) VL potential for subject 4. The intensities were normalized to the mean intensity in the frequency range covered by the wavelets with center frequencies from 107 to 247 Hz.

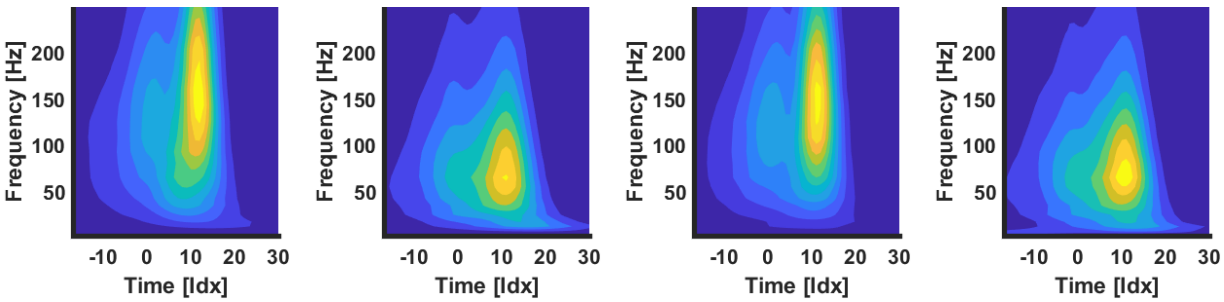

(a) (b) (c) (d)

Figure 4.15: Mean wavelet intensity patterns (WIP) for (a) VM current, (b) VL current, (c) VM potential, (d) VL potential for subject 8. The intensities were normalized to the mean intensity in the frequency range covered by the wavelets with center frequencies from 107 to 247 Hz.

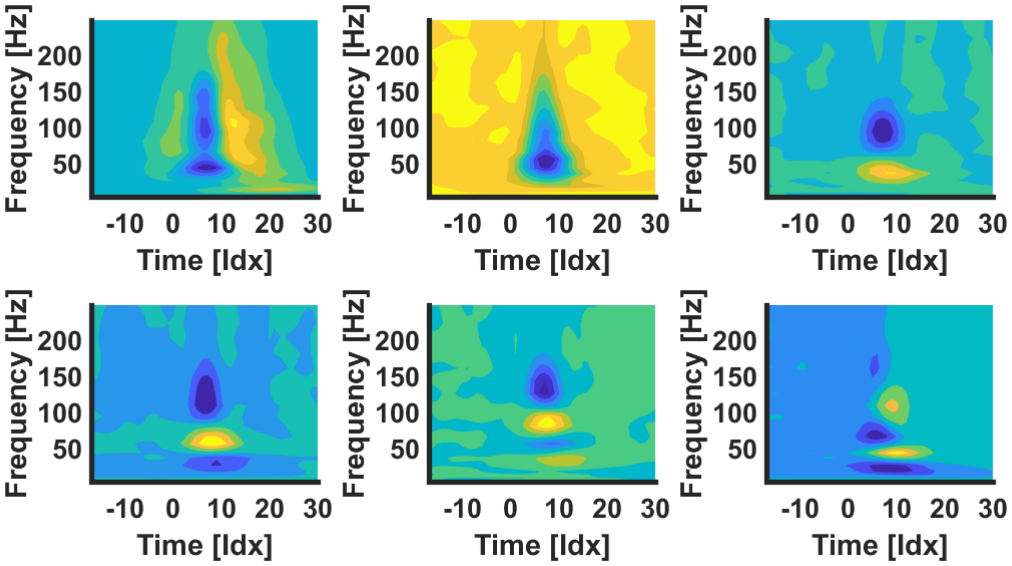

(a)

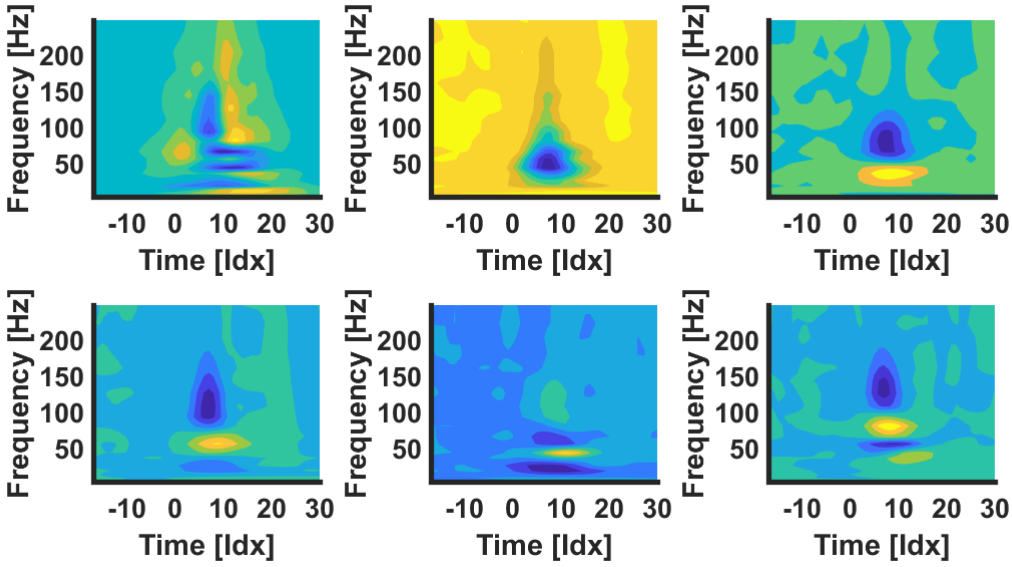

(b)

Figure 4.16: WIPs of the PPs of the VM data of subject 3 for (a) current and (b) potential measurements. In both examples the top left pattern shows the residual mean, it is needed to be able to reconstruct the mean. The residual mean is followed by the WIPs of the first five PPs. The maximal positive value is indicated in bright color and the maximal negative value is indicated in dark color. The vectors describing the PPs as well as the residual mean are all orthogonal to one another.

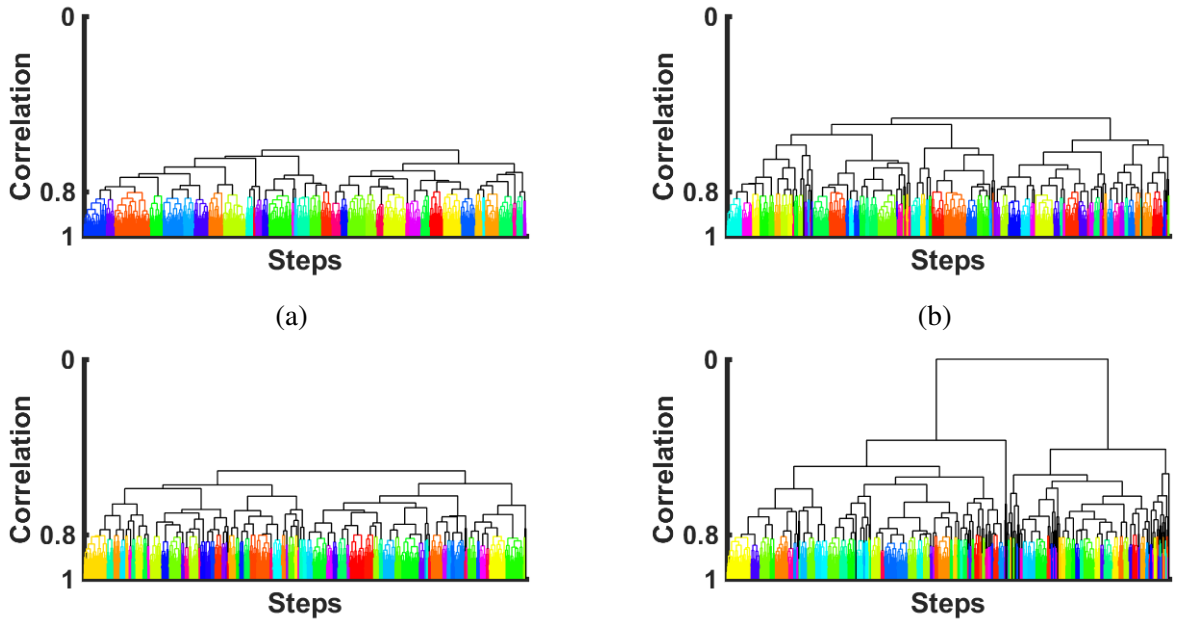

Figure 4.17: Hierarchical clustering of 1345 steps from subject 1 with current amplifier for (a) VM (38 clusters) and (c) VL (71 clusters), and for surrogate patterns of (b) VM (76 clusters) and of (d) VL (126 clusters).

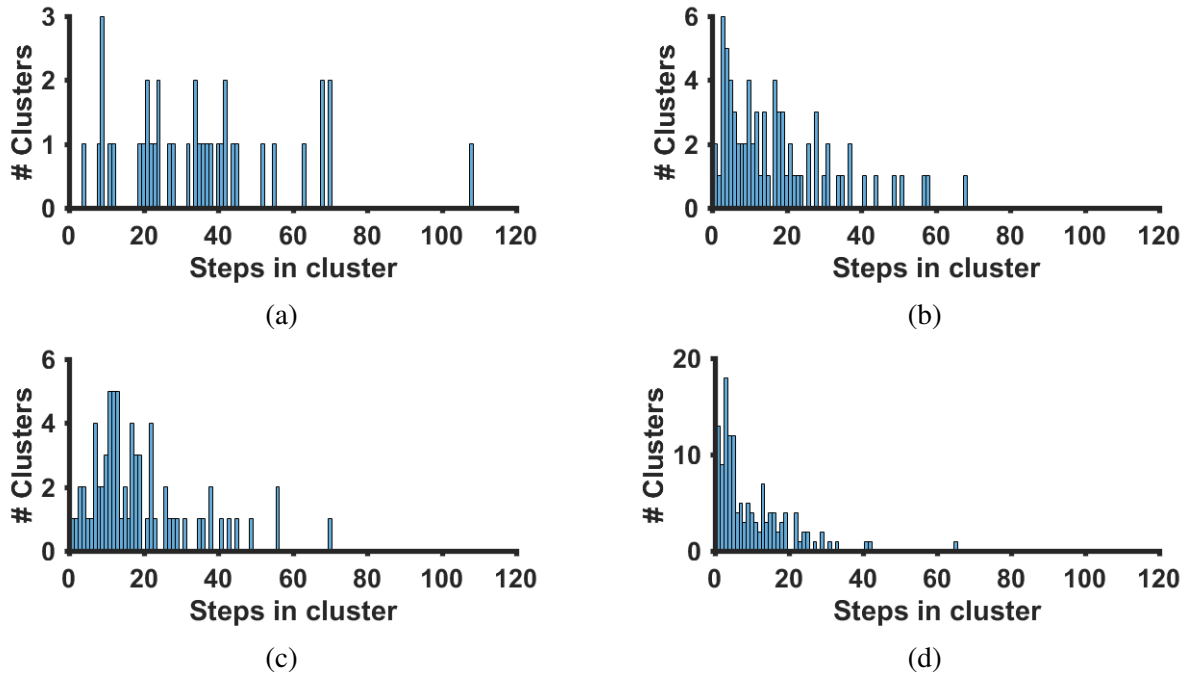

Figure 4.18: Histograms of subject 1 showing the number of clusters containing a certain number of steps per cluster for (a) VM and (c) VL, and for surrogate patterns of (b) VM and of (d) VL.

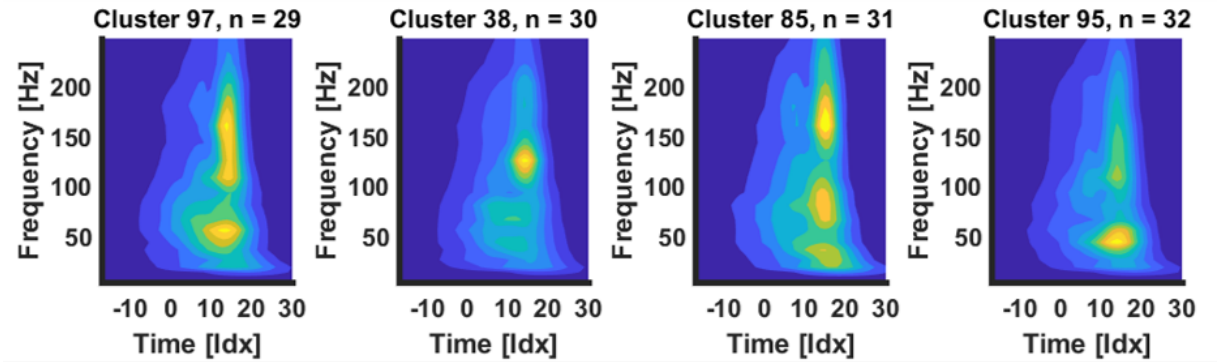

Figure 4.19: Mean WIPs of the four biggest clusters of subject 3, data measured from VL with current amplifier.

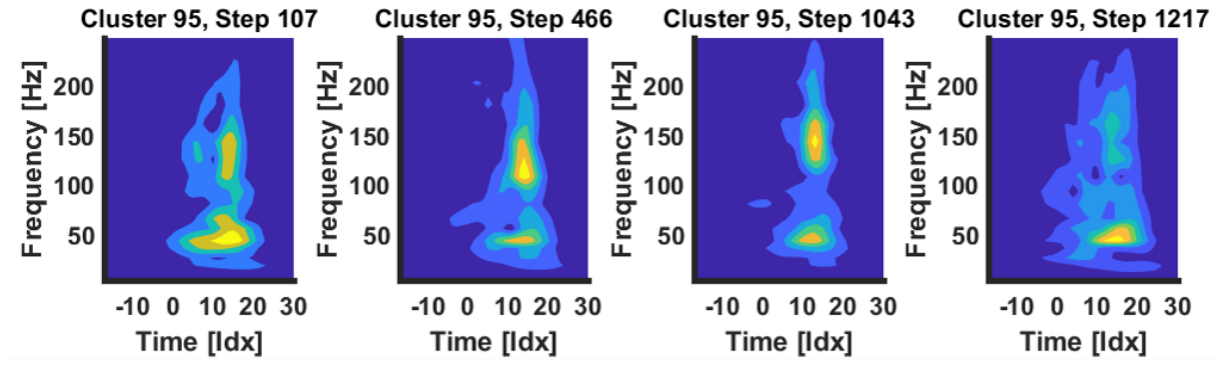

Figure 4.20: Four examples of WIPs from the biggest cluster of subject 3, data measured from VL with current amplifier.

Table 4.5: Clustering: current amplifier, VM

Subject	1	2	3	4	5	6	7	8	9	10	11	12	Mean
Steps	1345	1211	1245	1221	1258	1141	1343	1138	1382	1238	1374	1209	1259
PCs	37	44	43	41	45	55	30	53	35	32	55	55	44
NoClusters	38	26	57	43	46	50	78	98	73	14	131	153	67
MedianNoSteps	34	28	17	26	22	17	16	10	16	54	9	8	21
NoClusters_Sur	76	40	89	70	90	93	129	161	113	71	232	274	120
MedianNoSteps_Sur	13	19	9	13	10	8	7	5	9	5	4	3	9

Table 4.6: Clustering: current amplifier, VL

Subject	1	2	3	4	5	6	7	8	9	10	11	12	Mean
Steps	1345	1211	1245	1221	1258	1141	1343	1138	1382	1238	1374	1209	1259
PCs	39	31	49	38	38	30	32	48	30	43	45	50	39
NoClusters	71	19	98	50	57	57	40	98	93	62	87	116	71
MedianNoSteps	15	53	12	20	21	15	27	11	11	19	14	10	19
NoClusters_Sur	126	37	141	95	110	89	81	150	164	104	141	20	120
MedianNoSteps_Sur	7	25	7	10	7	9	11	5	6	9	8	4	9

Table 4.7: Clustering: potential amplifier, VM

Subject	1	2	3	4	5	6	7	8	9	10	11	12	Mean
Steps	1330	1209	1245	1197	1258	1142	1349	1139	1000	1233	1371	1178	1221
PCs	37	49	39	41	45	38	30	51	31	51	57	52	43
NoClusters	60	78	47	61	51	80	33	99	25	22	132	151	70
MedianNoSteps	17	14	20	18	20	11	36	10	27	45	10	7	20
NoClusters_Sur	110	124	80	105	88	208	76	161	49	49	212	282	129
MedianNoSteps_Sur	8	7	10	8	11	3	12	4	13	18	5	3	8

Table 4.8: Clustering: potential amplifier, VL

Subject	1	2	3	4	5	6	7	8	9	10	11	12	Mean
Steps	1330	1209	1245	1197	1258	1142	1349	1139	1000	1233	1371	1178	1221
PCs	40	31	44	41	38	28	33	47	29	41	49	48	39
NoClusters	91	50	75	75	65	50	32	58	34	70	99	106	67
MedianNoSteps	13	23	14	15	14	17	30	19	23	16	13	10	17
NoClusters_Sur	140	81	120	127	110	73	69	98	65	107	144	201	111
MedianNoSteps_Sur	7	11	8	7	8	10	14	8	10	9	7	4	9

4.3 Discussion

The results for the hardware comparison and the several analysis parts will be discussed in the following sections.

4.3.1 Comparison of amplifier systems

General signal characteristics

One goal of the project was to develop a new amplifier system that was able to measure EMG-currents in a bipolar way (Chapter 3). The new bipolar current amplifier and also the established bipolar potential amplifier were used in the running study in order to compare the results of the measurements (Section 4.1.3). The data shown in Fig. 4.9 reveals that both measurement systems were capable of measuring high quality EMG raw signals of VM and VL during running. An obvious difference of the signals from current and potential amplifiers in Fig. 4.9 is the signal amplitude. However, this is only due to the different output ranges, where the current amplifier was putting out signals between -1 and +1 V, and the potential amplifier sent signals between -4 and +4 V. Despite the lower output range of the current amplifier it was possible to adjust the amplification to obtain the best possible signal to noise ratio for each individual subject. The validity of the measurements with the current amplifier also becomes obvious when looking at the overall average wavelet spectra in Fig. 4.10. The spectra computed from the current and the potential signals show a very similar shape, with the exception that the current amplifier signals contain slightly more low frequency content. Considering the results shown in Fig. 4.10, one can assume that the EMG signals measured with both amplifier systems are in general very similar in terms of their frequency content.

Coherence with currents and potentials

According to Table 4.4, the highest coherence over all subjects in both amplifier systems is obtained in the frequency range between 5 and 60 Hz. The group of the subjects that showed a high average coherence with values higher than 0.2 is the same for both amplifiers (subjects 4, 5, 6, 7, and 9). Even though the values slightly differ between the two measurement systems, the order of the subjects with respect to the average coherence is the same comparing the amplifiers, except for subjects 7 and 9, who have switched positions in the ranking.

The same is true for the lower end of the coherence values: There are three subjects (3, 11, and 12) that have an average coherence of less than 0.1 in the current measurements and the same

subjects show very low values in the potential measurements, too. Exceptions are obtained for subjects 1, 2, 8, and 10, where the values between current and potential measurements have larger differences. Possible reasons for these exceptions will be discussed later.

Clustering with currents and potentials

The comparison of the results for PCA and clustering (Table 4.5, Table 4.6, Table 4.7, and Table 4.8) confirms the impression of very similar results for the two amplifier systems: According to the results of the PCA the average number of PPs that were necessary to describe 90 % of the variance of the data was for both amplifier systems close to 43 for VM and 39 for VL. The same is true for the number of clusters that were obtained in the WIPs of the original running steps. This value was on average around 69 for both muscles measured by both amplifier systems.

Considering the underwater measurements reported in Section 3.6, the similar results of current and potential measurements might be surprising. All subjects were sweating during the running exercise and sweat on the skin has a similar influence on the signal quality as the surrounding water in the pilot tests. The underwater measurements, however, were a very extreme case, where the electrodes as well as the connections were completely under water and therefore definitely short circuited. In case of the running study, the sweat might not have been distributed as homogeneously as the water, so the two measurement points in the bipolar electrode were not exposed to a short circuit. If bipolar electrodes with a closer inter-electrode distance were used, the problem of cross talk could become more serious when using potential amplifiers.

4.3.2 Coherence analysis

In summary the coherence analysis for the data of the presented running study gives clear evidence, that VM and VL work in a synchronized way during running. Coherence is therefore one way to reveal the structure and non-randomness that is present in EMG signals.

Significant coherence in two frequency bands

The results for the coherence analysis presented in Fig. 4.12, Fig. 4.13, and in Table 4.4 show that with respect to the computed reference coherence of non-synchronized signals there was a significant coherence of VM and VL during running. This result indicates the appearance of similar EMG signal patterns in different muscles that are involved in running and thus supports the first hypothesis (Chapter 1).

Significant coherence was obtained in both of the frequency bands of 5 to 60 Hz and 60 to 250 Hz in both measurement systems. Fig. 4.12 shows a pronounced peak of the average coherence of all subjects in the low frequency range, that goes along with results reported in previous publications, where the movement task was cycling [CM16] or squatting [Moh15]. Task-dependent intermuscular motor unit synchronization using EMG-currents was also obtained in vertical calf rising movments [vT14a]. In these articles, no relevant coherence was observed in frequencies higher than 100 Hz, whereas the results in this project clearly also show a significant coherence in the area around 180 Hz for all subjects. A reason for this additional peak in the coherence spectrum could lie in the different characteristics of the movements performed in the previous studies and running in this project. Vertical calf rising [vT14a], squatting [Moh15] and ergometer cycling [CM16] are all movements that are rather stationary in the sense that the subjects were standing or sitting on the same spot when performing the movement. In treadmill running, however, the whole body of the subject was in motion. Therefore, the high frequency coherence of the muscles could reflect some sort of fine tuning of the muscles that is necessary to keep the body in balance by using a faster type of motor units.

Subject dependency for coherence

The results presented in Section 4.2.2 also show that coherence is a very subject specific phenomenon. Some of the subjects, like in the example in Fig. 4.11, show a very distinct coherence in the two previously mentioned frequency bands. Others have a less pronounced high frequency peak and some a spectrum with the two peaks but with a magnitude of the coherence values that is barely higher than the significance border (Table 4.4).

One possible explanation of the difference in coherence between subjects could be a relation to the individual running experience. Comparing the information the subjects gave about their typical running distance per week in Table 4.2 with the coherence results in Table 4.4, however, does not yield a clear correlation between these two values: The subject with the most km per week, subject 11, showed very low coherence values, but subject 8, who reported no regular running training, showed low coherence as well. There are also examples the other way around for very high coherence values: Subjects 6 and 7 were among those with the highest average coherence values, where subject 7 reported to run 20 km per week but subject 6 does not practice running at all. The subject dependence of coherence was also reported by the authors of [CM16] and [Nan14] and possible factors for the coherence of muscle activity still have to be further investigated.

General remarks

The results of the coherence analysis in this thesis now add running as another important human movement, where the synchronization of muscles that are participating in the same task could be shown. In the quoted articles, the current based EMG measurements were done with monopolar amplifiers, which was reasonable with respect to the characteristics of the respective movement tasks. The results for EMG-currents for running in this project were only possible due to the use of a bipolar current amplifier that was providing cancellation of noise and motion artifacts as described in Chapter 3.

4.3.3 Clustering

Outgoing from the findings of the coherence analysis it was reasonable to look further into the signals that can be recorded from the single muscles and try to find repeated characteristics that show up within one muscle over time. In Chapter 1 it was hypothesized that every human would show an individual finite number of EMG signal patterns within one muscle over time. According to the results in Table 4.5, Table 4.6, Table 4.7, and Table 4.8, this hypothesis can be supported: The number of patterns is finite as there are certain clusters of similar patterns. For all subjects both measurements with current and potential amplifiers from VM and VL showed a number of clusters of WIPs of running steps that was clearly lower than the number of steps they performed. The results show that the number of clusters is highly subject dependent and in a wide range of 14 clusters for VM in the current measurement of subject 10 and 153 clusters in the same condition for subject 12.

Frequency spectra as structural elements

It is necessary to understand the reason for the grouping of the data by looking at the specific characteristics and structures of the single clusters. The most important structural elements of the WIPs are several distinct frequency bands that are activated. The average WIPs of two subjects in Fig. 4.14 and Fig. 4.15 give a good impression of these bands: Subject 4 in Fig. 4.14 shows dominant intensities around 65 Hz and for the current measurements (Fig. 4.14a and Fig. 4.14b) also a lower frequency component around 40 Hz and 25 Hz. In contrast subject 8 shows distinctly higher frequencies for VM (Fig. 4.15a and Fig. 4.15c) and for VL the main frequencies are more widely spread between 50 and 100 Hz (Fig. 4.15b and Fig. 4.15d).

The named frequency bands become even more apparent in the WIP-representation of the PPs. The PPs are computed from the principal component vectors of the whole EMG data set from one

measurement condition. Hence the PPs represent areas in the pattern that contribute together, thus in a correlated way to the final WIP. Examples for this are presented in Fig. 4.16: The first PP indicates a dominant band between 50 and 60 Hz. Distinct intensities around 40 and 100 Hz are obvious in the second PP. Finally, the very low frequency component around 25 Hz is contributed by the principal patterns 3 - 5.

The mentioned major 4 frequency components (25 Hz, 40 Hz, 65 Hz, and around 100 Hz) are the structural elements of the patterns. The way how the EMG intensity in these regions is distributed decides, which cluster a pattern of a single step can be assigned to. These distinct frequency bands could be resolved by an adaption of the parameters for the wavelet transform presented in [vT00] towards a higher resolution in low frequencies.

Explanations for the appearance of the distinct frequency bands can be found in the literature: The low frequency band could be caused by the clustering of MUs at specific time points as a result of common synaptic input to motor neurons [Lai15]. On average the frequency band between 35 and 100 Hz contributes most of the intensity to the WIPs (Fig. 4.14 and Fig. 4.15). According to Merletti et al. [Mer97] this frequency band represents the power spectrum of the majority of MUAPs. It is altered by peripheral fatigue and sensitive to changes in muscle fiber conduction velocity. The high frequencies that were obtained in subject 8 (Fig. 4.15a and Fig. 4.15c) can be explained with a special type of fast MUs described in [Wak04]. After all, the power spectrum of an EMG during running is a result of multiple processes that each affect the power spectrum in different frequency bands.

Significance of clusters

The clustering result of the surrogate signals underlines the significance of the clusters that were found in the original EMG signals: For all conditions the number of clusters that were determined based on artificial surrogate signals was always at least 50 % and up to 500 % higher than the number of clusters determined from the WIPs based on real EMG signals. More insight about the difference between real and surrogate signals is gained through a comparison of the respective cluster sizes (Fig. 4.18), meaning the median number of steps that were assigned to each cluster. Based on the Wilcoxon rank sum test the median values for the real signals are significantly higher than those of the surrogate signals for all subjects in all four conditions. The WIPs of the real EMG signals were thus grouped into significantly larger clusters compared to the surrogate signals. Hence, the surrogate signals did not show sufficient structure to form big groups.

This result shows that the WIPs of EMG signals are not consisting of a random combination of intensity values, but have a certain structure that was repeatedly observed. In the previous

section it was shown that this structure is related to different frequency bands that are activated in different steps. These structures are the basis for assigning the different steps into meaningful groups. Considering the differences to the clustering result of the surrogate signals, one could conclude that the activation strategy of the running steps is centrally predefined and that certain template patterns are activated when needed. Even though there is some variability between the mean patterns of the clusters, for example for subject 3 in Fig. 4.19, a combination of the distinct structural elements is always visible. A possible explanation of the variability is the need for fine adjustments of the activation pattern to stabilize gait.

Besides the variability of the patterns in the different clusters, the consistency within the clusters is important for a meaningful clustering result. The sample WIPs from the biggest cluster in the EMG-current data of subject 3's VL in Fig. 4.20 reveal, that within this cluster the patterns of the several steps do in fact look very similar and show the same activation of frequency bands at the same points in time. The steps shown in Fig. 4.20 did not happen in a short time sequence, but happened at the very beginning (step 107) and almost at the end (step 1217) of the running trial of this subject. This observation confirms the idea of a predefined activation strategy, from which certain patterns are activated when needed.

Subject dependency for clustering

Similar to the results for the coherence, also the question regarding the number of task-specific EMG signal patterns within one muscle, needs to be answered individually for every subject. Table 4.5, Table 4.6, Table 4.7, and Table 4.8 show a high range of number of clusters over all measurements. As for coherence, also for the number of clusters in the EMG signals there is no obvious trend regarding a correlation between running experience and number of clusters. There are subjects with higher numbers of clusters (subject 8 and subject 11) that have totally different running experience. On the other hand, some subjects had a lower number of clusters (subject 2 and subject 7) despite a big difference in the average km covered per week. As one cannot make a clear statement about the general meaning of the clustering results, it is most likely more reasonable to treat the results only within the single subjects. It could for example be interesting to see how the clustering of WIPs changes in the case of certain interventions like different running shoes, different running speeds or different ground surfaces.

Limitations

The presented results have certain limitations. In order to proof a general valid number of EMG patterns for an individual subject, one would have to find a way to produce repeatable results.

A slight indication of repeatability can be drawn from the comparison of the measurements with current and potential amplifiers. As described in Section 4.1.3 the measurements with both signal acquisition systems were executed right after another, the electrodes were not moved and considering the non-fatiguing task of steady state running, a similar result for parameters like number of clusters and median cluster size can be expected for both measurements. The results, however, show some differences for comparisons of the same muscles with the two amplifiers. At least the relation between the number of clusters determined for VM and VL stays the same for 9 of the subjects: If for these subjects the number of clusters in VM was higher than in VL for the current measurement, the same trend was observed in the potential measurement and the other way around. Besides that, the difference between the absolute values for the clustering result do not indicate a very high repeatability when comparing current and potential measurements.

One limiting factor here is identified in the decision how to set the cut-off value for the maximum dissimilarity within a cluster. In this thesis the value was set to 0.2, which corresponds to a minimum correlation coefficient of 0.8 between patterns that were assigned to the same group. If the cut-off was set much lower the cluster sizes become small, if the cut-off is too high, only a few groups will be isolated, that are not meaningful anymore. A dynamic adaption of the cut-off value, with respect to the several given input parameters could lead to some kind of normalization of the results. Thus, the result in this stage cannot yet be used to decide about the absolute number of predefined WIPs for a subject. However, the presented results clearly suggest that there are repetitive WIPs that are distinctly different (Fig. 4.19 and Fig. 4.20).

Chapter 5

Conclusion and outlook

The purpose of this thesis was to answer questions regarding the non-randomness of EMG signals and if the human body uses predefined muscle activation patterns, or if the EMG signals for every single step in running are unique. The task to answer these questions was tackled with attempts to contribute to EMG research on the data acquisition and on the data analysis side.

The development of a bipolar version of the previously used monopolar current amplifier allowed the measurement of EMG-currents during running. The pilot study with underwater measurements, as well as the results of the running study, gave proof of the validity of the new hardware for the application in different environments in sports and healthcare, where water and sweat, as well as impact forces and motion of body segments have to be dealt with. Even though the results for both amplifier systems in the running study do not show major differences, the current amplifier would reveal its advantages in possible underwater studies (swimming, physiotherapy, etc.) or in case of a closer inter-electrode distance. In an early stage of the project the goal was to use electrodes with an inter-electrode distance of 5 mm which would yield a more precise measurement of the MUAP differential. The potential issue of intra-electrode cross-talk caused by sweat on the skin would then probably be a more severe problem than it was for the regular electrodes used in the present study. Successful attempts to build custom-made reusable 3D-printed electrodes with short inter-electrode distance were undertaken in the course of this project, however, the limited time did not allow to make them feasible for the use in the running study. The use of a smaller inter-electrode distance and hence the exploitation of the advantage of the bipolar current amplifier would therefore be one objective for future studies.

In the signal analysis part, many methods that have been successfully used in previous EMG studies (coherence, PCA, wavelet transform) were applied to running and further developed with the goal to find groups of EMG signal patterns showing up within one muscle when performing

a repeated task. Outgoing from the findings in the coherence analysis, which revealed the synchronization of VM and VL during running, signals within the single muscles were investigated regarding repeatedly used muscle activation patterns. The results of the applied clustering algorithm in this study give good reasons for the assumption that the activation strategy of the running steps is centrally predefined and that patterns from certain groups are activated when needed. It has been shown that the differences between those groups are located in various frequency bands and thus it is important to further improve the understanding of how the physiological properties, that control the motor task, translate into these bands. For a general determination, for example of the absolute number of predefined patterns, a more exhaustive review of available algorithmic solutions is necessary. The use of PCA and hierarchical clustering is only one way for detecting structures in the intensity patterns. Among others, independent component analysis and Kohonen maps would be further possible methods.

Once possibilities are determined that allow reliable and repeatable measurements of some sort of default activation strategy of an individual, further studies could investigate a change of this strategy under the influence of different running speed, different running shoes or in the context of recovery from injuries. Possible applications would thus be the measurement of fatigue, running shoe recommendations or the quantification of a rehabilitation process. Taking these options into consideration, the present study describes some important innovative approaches that may contribute to the further development of technologies in healthcare and sports.

Appendix A

Glossar

Ag	Argentum / Silver
ASIS	Anterior superior iliac spine
Cl	Chloride
CMR	Common mode rejection
CMRR	Common mode rejection ratio
DC	Direct current
ECG	Electrocardiography
EMG	Electromyography
FFT	Fast Fourier transform
IA	Instrumentation amplifier
K	Kalium / Potassium
MU	Motor unit
MUAP	Motor unit action potential
Na	Natrium / Sodium
OPAMP	Operational amplifier
PCA	Principal component analysis
PCB	Printed circuit board
PP	Principal pattern
STD	Standard deviation
TCA	Transconductance amplifier
TIA	Transimpedance amplifier
TKA	Total knee arthroplasty
VL	Vastus lateralis muscle
VM	Vastus medialis muscle
WIP	Wavelet intensity pattern

Appendix B

Patents

B.1 US5513651

Title	Integrated movement analyzing system
Publication Number	US5513651
Publication Date	1996-05-07
Inventor(s)	MaryRose Cusimano, Michael A. Potorti
Current Assignee	OKTX LLC Insight Diagnostics Inc.
Abstract	An integrated movement analyzing system that utilizes surface electromyography in combination with range of motion and functional capacity testing to monitor any muscle group in the human body. The system consists of an integrated movement analyzer that receives inputs from up to 32 channels of surface EMG electrodes, a range of motion arm (ROMA) having six degrees of freedom, and a functional capacity sensor (FGS) having one output channel. When performing upper and lower back testing, the ROMA is connected between the patient's upper back and lower back by a shoulder harness and a waist belt. For cervical testing, the ROMA is connected between the patient's head and upper back by a cervical cap and the shoulder harness. The output of the IMA is provided via an analog to digital converter to a computer. The computer in combination with a software program produces comparative analytical data which is primarily in the form of graphic plots.

B.2 US5277197

Title	Microprocessor controlled system for unsupervised EMG feedback and exercise training
Publication Number	US5277197
Publication Date	1994-01-01
Inventor(s)	John Church, William Hassel
Current Assignee	Encore Medical Asset Corp
Abstract	An exercise training system for prompting a user for stereotyped exercise and recording the intensity of the exercise, the training system consisting of an electromyographic sensor member which produces a rectified and time averaged signal forming a muscle force signal, the sensor member being provided with at least one electrode that is positioned adjacent to the user's muscle group for indicating muscle force of that muscle group, and a control member having a clock for measuring time intervals, and an alerting member for alerting the user that an exercise period has started as determined by the clock for a predetermined time interval loaded into the control means, whereby the user in response to the alerting member contracts and relaxes a predetermined muscle group and the muscle force used in the exercise is sensed by the electromyographic sensor.

B.3 US8170656

Title	Wearable electromyography-based controllers for human-computer interface
Publication Number	US8170656
Publication Date	2012-05-01
Inventor(s)	Desney Tan, T. Scott Saponas, Dan Morris, Jim Turner
Current Assignee	Microsoft Technology Licensing LLC
Abstract	A 'Wearable Electromyography-Based Controller' includes a plurality of Electromyography (EMG) sensors and provides a wired or wireless human-computer interface (HCl) for interacting with computing systems and attached devices via electrical signals generated by specific movement of the user's muscles. Following initial automated self-calibration and positional localization processes, measurement and interpretation of muscle generated electrical signals is accomplished by sampling signals from the EMG sensors of the Wearable Electromyography-Based Controller. In operation, the Wearable Electromyography-Based Controller is donned by the user and placed into a coarsely approximate position on the surface of the user's skin. Automated cues or instructions are then provided to the user for fine-tuning placement of the Wearable Electromyography-Based Controller. Examples of Wearable Electromyography-Based Controllers include articles of manufacture, such as an armband, wristwatch, or article of clothing having a plurality of integrated EMG-based sensor nodes and associated electronics.

Appendix C

Mean wavelet intensity patterns

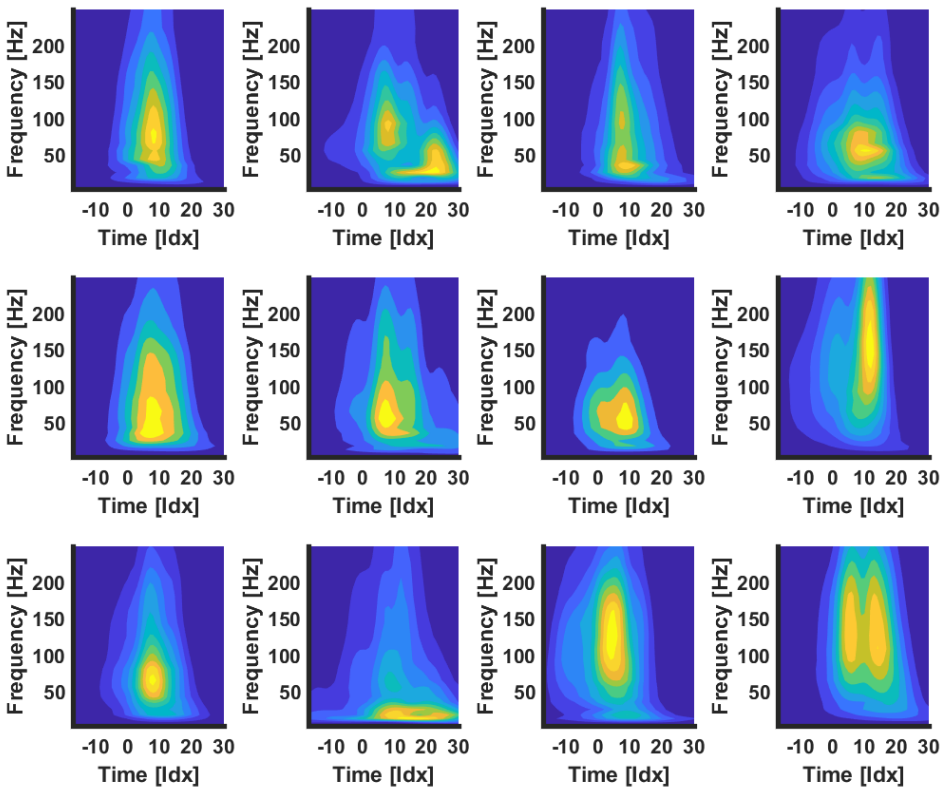

Figure C.1: Mean wavelet intensity patterns (WIP) for **current** measurements from **VM** for 12 subjects. The subject index is ascending from left to right and top to bottom. The intensities were normalized to the mean intensity in the frequency range covered by the wavelets with center frequencies 107 to 247 Hz.

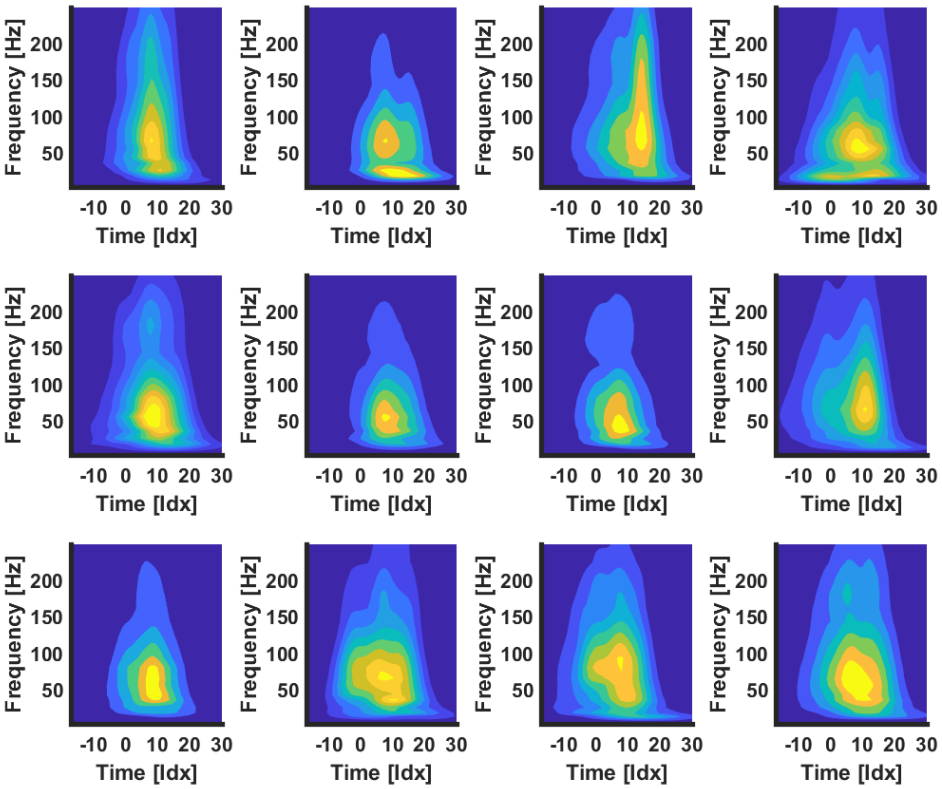

Figure C.2: Mean wavelet intensity patterns (WIP) for **current** measurements from **VL** for 12 subjects. The subject index is ascending from left to right and top to bottom. The intensities were normalized to the mean intensity in the frequency range covered by the wavelets with center frequencies 107 to 247 Hz.

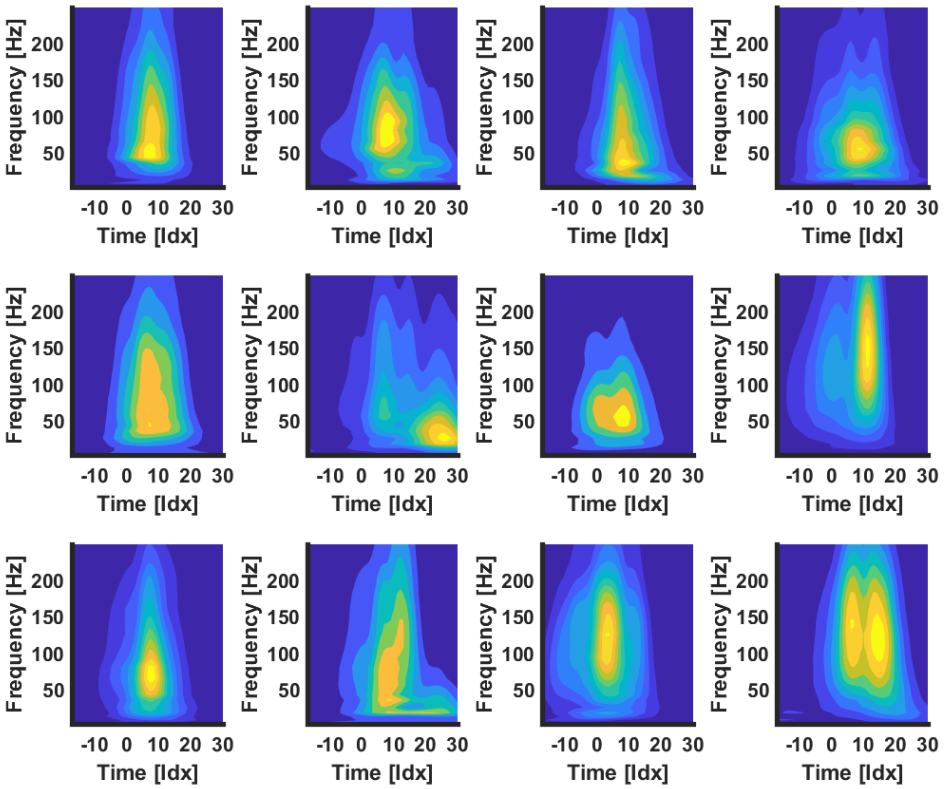

Figure C.3: Mean wavelet intensity patterns (WIP) for **potential** measurements from **VM** for 12 subjects. The subject index is ascending from left to right and top to bottom. The intensities were normalized to the mean intensity in the frequency range covered by the wavelets with center frequencies 107 to 247 Hz.

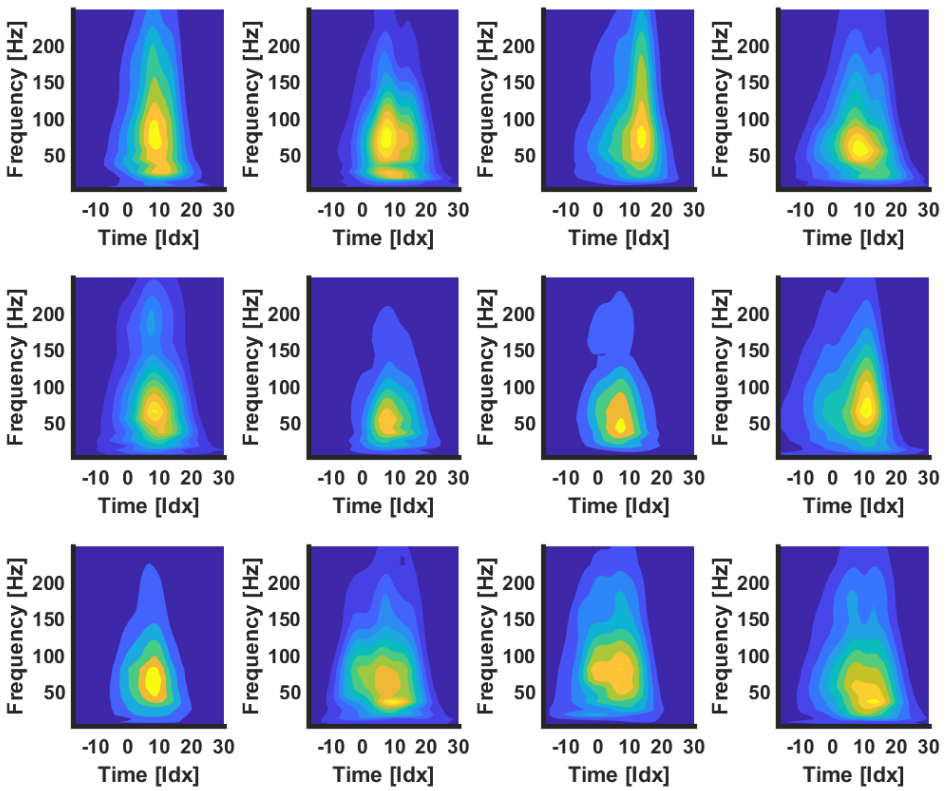

Figure C.4: Mean wavelet intensity patterns (WIP) for **potential** measurements from **VL** for 12 subjects. The subject index is ascending from left to right and top to bottom. The intensities were normalized to the mean intensity in the frequency range covered by the wavelets with center frequencies 107 to 247 Hz.

List of Figures

List of Tables

Bibliography

[AE12] M. Abdoli-Eramaki, C. Damecour, J. Christenson, and J. Stevenson. The effect of perspiration on the semg amplitude and power spectrum. *Journal of Electromyography and Kinesiology*, 22(6):908–913, 2012.

[Ame06] S. Amershi, C. Conati, and H. McLaren. Using feature selection and unsupervised clustering to identify affective expressions in educational games. In *Workshop in Motivational and Affective Issues in ITS, 8th International Conference on Intelligent Tutoring Systems, Jhongli, Taiwan*, 2006.

[Ban12] S. Bandyopadhyay and S. Saha. *Unsupervised classification: similarity measures, classical and metaheuristic approaches, and applications*. Springer Science & Business Media, 2012.

[Bar15] K. Barnes and A. Kilding. Running economy: measurement, norms, and determining factors. *Sports medicine-open*, 1(1):8, 2015.

[Bis06] C. M. Bishop. *Pattern recognition and machine learning*. Springer, 2006.

[Chr99] C. I. Christodoulou and C. S. Pattichis. Unsupervised pattern recognition for the classification of emg signals. *IEEE Transactions on Biomedical Engineering*, 46(2):169–178, 1999.

[CM16] D. Comaduran Marquez. *Design and development of a multichannel current-EMG system for coherence analysis*. (Unpublished Master Thesis). Unversity of Calgary, Canada., 2016.

[CR16] V. Cregan-Reid. Why running is fast becoming the most popular way to exercise. *The Independent*, 2016.

[Dev17] Molecular Devices. What is an action potential? https://www.moleculardevices.com/what-action-potential, 2017. Accessed: 2017-10-29.

[DL93] C. J. De Luca, A. M. Roy, and Z. Erim. Synchronization of motor-unit firings in several human muscles. *Journal of Neurophysiology*, 70(5):2010–2023, 1993.

[DL97] C. J. De Luca. The use of surface electromyography in biomechanics. *Journal of applied biomechanics*, 13(2):135–163, 1997.

[DSC10] R. G. Da Silva Carvalho, C. F. Amorim, L. H. R. Perácio, H. F. Coelho, A. C. Vieira, H.-J. K. Menzel, and L. A. Szmuchrowski. Analysis of various conditions in order to measure electromyography of isometric contractions in water and on air. *Journal of Electromyography and Kinesiology*, 20(5):988–993, 2010.

[Dud12] R. O. Duda, P. E. Hart, and D. G. Stork. *Pattern classification*. John Wiley & Sons, 2012.

[End14] H. Enders, V. von Tscharner, and B. M. Nigg. Neuromuscular strategies during cycling at different muscular demands. *Medicine and science in sports and exercise*, 47, 11 2014.

[Eno88] R. M. Enoka. *Neuromechanical basis of kinesiology.* ERIC, 1988.

[Far93] S. F. Farmer, F. D. Bremner, D. M. Halliday, J. R. Rosenberg, and J. A. Stephens. The frequency content of common synaptic inputs to motoneurones studied during voluntary isometric contraction in man. *The Journal of physiology*, 470(1):127–155, 1993.

[Geo03] A. Georgakis, L. K. Stergioulas, and G. Giakas. Fatigue analysis of the surface emg signal in isometric constant force contractions using the averaged instantaneous frequency. *IEEE Transactions on Biomedical Engineering*, 50(2):262–265, 2003.

[Gül05] N. F. Güler and S. Koçer. Use of support vector machines and neural network in diagnosis of neuromuscular disorders. *Journal of medical systems*, 29(3):271–284, 2005.

[Her99] H. J. Hermens, B. Freriks, R. Merletti, D. Stegeman, J. Blok, G. Rau, C. Disselhorst-Klug, and G. Hägg. European recommendations for surface electromyography. *Roessingh research and development*, 8(2):13–54, 1999.

[Kon06] P. Konrad. The abc of emg - a practical introduction to kinesiological electromyography. 2006.

[Kun15] G. Kuntze, V. von Tscharner, C. Hutchison, and J. L. Ronsky. Multi-muscle activation strategies during walking in female post-operative total joint replacement patients. *Journal of Electromyography and Kinesiology*, 25(4):715–721, 2015.

[Lai15] C. M. Laine, E. Martinez-Valdes, D. Falla, F. Mayer, and D. Farina. Motor neuron pools of synergistic thigh muscles share most of their synaptic input. *Journal of Neuroscience*, 35(35):12207–12216, 2015.

[Lau16] J. Lauber. *Underwater Electrocardiography*. (Master Thesis). Friedrich-Alexander-Universität Erlangen-Nürnberg, Germany., 2016.

[Mat17a] Matlab Documentation MathWorks. corrcoef - correlation coefficients. `https://de.mathworks.com/help/matlab/ref/corrcoef.html`, 2017. Accessed: 2017-10-19.

[Mat17b] Matlab Documentation MathWorks. linkage - agglomerative hierarchical cluster tree. `https://de.mathworks.com/help/stats/linkage.html`, 2017. Accessed: 2017-10-19.

[Mel05a] R. Mellor and P. W. Hodges. Motor unit synchronization between medial and lateral vasti muscles. *Clinical neurophysiology*, 116(7):1585–1595, 2005.

[Mel05b] R. Mellor and P. W. Hodges. Motor unit syncronization is reduced in anterior knee pain. *The Journal of pain*, 6(8):550–558, 2005.

[Mer97] R. Merletti and L. R. Conte. Surface emg signal processing during isometric contractions. *Journal of Electromyography and Kinesiology*, 7(4):241–250, 1997.

[Moh15] M. Mohr, M. Nann, V. von Tscharner, B. Eskofier, and B. M. Nigg. Task-dependent intermuscular motor unit synchronization between medial and lateral vastii muscles during dynamic and isometric squats. *PloS one*, 10(11):e0142048, 2015.

[Mot93] C. D. Motchenbacher and J. A. Connelly. *Low noise electronic system design*. Wiley, 1993.

[Mun87] C. F. Munro, D. I. Miller, and A. J. Fuglevand. Ground reaction forces in running: a reexamination. *Journal of biomechanics*, 20(2):147–155, 1987.

[Nan14] M. Nann. *Synchronization of monopolar EMG-currents between the vastii muscles during fatiguing squat movements*. (Master Thesis). Friedrich-Alexander-Universität Erlangen-Nürnberg, Germany., 2014.

[Nig10] B. M. Nigg. *Biomechanics of sport shoes*. University of Calgary, 2010.

[Nin15] Y. Ning, X. Zhu, S. Zhu, and Y. Zhang. Surface emg decomposition based on k-means clustering and convolution kernel compensation. *IEEE journal of biomedical and health informatics*, 19(2):471–477, 2015.

[Nov98] T. F. Novacheck. The biomechanics of running. *Gait & posture*, 7(1):77–95, 1998.

[Rai04] A. Rainoldi, C. Cescon, A. Bottin, R. Casale, and I. Caruso. Surface emg alterations induced by underwater recording. *Journal of electromyography and Kinesiology*, 14(3):325–331, 2004.

[Ram09] X. Ramus. Transimpedance considerations for high-speed amplifiers. *Application Report SBOA122. Texas Instruments*, 2009.

[Rea06] M. B. I. Reaz, M. S. Hussain, and F. Mohd-Yasin. Techniques of emg signal analysis: detection, processing, classification and applications. *Biological procedures online*, 8(1):11–35, 2006.

[Ros89] J.R. Rosenberg, A.M. Amjad, P. Breeze, D.R. Brillinger, and D.M. Halliday. The fourier approach to the identification of functional coupling between neuronal spike trains. *Progress in biophysics and molecular biology*, 53(1):1–31, 1989.

[Sem02] J. G. Semmler. Motor unit synchronization and neuromuscular performance. *Exercise and sport sciences reviews*, 30(1):8–14, 2002.

[Sil09] D. U. Silverthorn. *Physiologie*. Pearson Deutschland GmbH, 2009.

[Spe08] E.-J. Speckmann, J. Hescheler, and R. Köhling. *Physiologie*, volume 5. Urban & Fischer, 2008.

[Tay90] R. Taylor. Interpretation of the correlation coefficient: a basic review. *Journal of diagnostic medical sonography*, 6(1):35–39, 1990.

[Tex15] Texas Instruments. *INA12x Precision, Low Power Instrumentation Amplifiers*, October 2015. Rev. C.

[Tie16] U. Tietze and C. Schenk. *Halbleiterschaltungstechnik*, volume 15. Springer, 2016.

[vT00] V. von Tscharner. Intensity analysis in time-frequency space of surface myoelectric signals by wavelets of specified resolution. *Journal of Electromyography and Kinesiology*, 10(6):433–445, 2000.

[vT02] V. von Tscharner. Time–frequency and principal-component methods for the analysis of emgs recorded during a mildly fatiguing exercise on a cycle ergometer. *Journal of Electromyography and Kinesiology*, 12(6):479–492, 2002.

[vT03a] V. von Tscharner and B. Goepfert. Gender dependent emgs of runners resolved by time/frequency and principal pattern analysis. *Journal of Electromyography and Kinesiology*, 13(3):253–272, 2003.

[vT03b] V. von Tscharner, B. Goepfert, and B. M. Nigg. Changes in emg signals for the muscle tibialis anterior while running barefoot or with shoes resolved by non-linearly scaled wavelets. *Journal of biomechanics*, 36(8):1169–1176, 2003.

[vT09] V. von Tscharner. Spherical classification of wavelet transformed emg intensity patterns. *Journal of Electromyography and Kinesiology*, 19(5):e334–e344, 2009.

[vT13] V. von Tscharner, C. Maurer, F. Ruf, and B. M. Nigg. Comparison of electromyographic signals from monopolar current and potential amplifiers derived from a penniform muscle, the gastrocnemius medialis. *Journal of Electromyography and Kinesiology*, 23(5):1044–1051, 2013.

[vT14a] V. von Tscharner. Task dependent synchronization of motor units of the medial gastrocnemius muscle revealed in emg-currents. *J Exerc Sports Orthop 1 (1): 7*, 2014.

[vT14b] V. von Tscharner, C. Maurer, and B. M. Nigg. Correlations and coherence of monopolar emg-currents of the medial gastrocnemius muscle in proximal and distal compartments. *Frontiers in physiology*, 5, 2014.

[Wak04] J. M. Wakeling and A. I. Rozitis. Spectral properties of myoelectric signals from different motor units in the leg extensor muscles. *Journal of Experimental Biology*, 207(14):2519–2528, 2004.

[Whi14] J. W. Whitting and V. von Tscharner. Monopolar electromyographic signals recorded by a current amplifier in air and under water without insulation. *Journal of Electromyography and Kinesiology*, 24(6):848–854, 2014.

[Wol96] W. M. Wolf. The emg as a window to the brain: signal processing tools to enhance the view. In *Advances in processing and pattern analysis of biological signals*, pages 339–356. Springer, 1996.